

Methods for Pseudoscalar Flavour-Singlet Mesons with Staggered Fermions

Eric B. Gregory, Alan C. Irving, Chris M. Richards

*Theoretical Physics Division, Department of Mathematical Sciences,
University of Liverpool, Liverpool L69-7ZL, United Kingdom*

Craig McNeile

*Department of Physics and Astronomy,
The Kelvin Building, University of Glasgow,
Glasgow G12-8QQ, United Kingdom*

(Dated: September 4, 2021)

Abstract

We present the first 2+1 flavour lattice QCD calculations of pseudoscalar flavour-singlet propagators using improved staggered fermions. We explore the relevant techniques and discuss prospects for the larger scale studies now in progress. The disconnected correlator is shown to have a highly non-Gaussian distribution and reliable estimates of the errors require care.

PACS numbers: 11.15.Ha, 12.38.Gc, 14.40.Aq

I. INTRODUCTION

The high mass of the η' meson relative to the light pseudoscalar mesons is thought to be due to topology and the complexities of the QCD vacuum [1, 2]. The mass of the η' meson is a clear experimental signal of the complexities of the QCD vacuum that are normally obscured by confinement, so a first principles calculation of the mass would be an important milestone in taming non-perturbative QCD. A robust first-principles calculation of the spectrum of the η/η' system should help shed light on the workings of the fermion sea, and the mechanism by which quark loops elevate the mass of the singlet meson above that of the octet meson [1, 2].

The computation of the mass of the η' meson has always been one of the goals of the program of hadron spectroscopy from lattice QCD calculations. There have been many lattice studies that have computed the mass spectrum of pseudoscalar flavour-singlet mesons with $N_f = 2$ flavours of fermions [3, 4, 5, 6, 7, 8, 9, 10, 11]. Recently the JLQCD/CP-PACS collaboration reported on a preliminary calculation of the η and η' mesons with 2+1 flavours of Wilson fermions [12] .

Improved staggered fermions have provided some of the most impressive results in hadron spectroscopy for flavour non-singlet quantities [13, 14]. The next stage is to use improved staggered fermions to compute the mass spectrum of light singlet pseudoscalar mesons. Improved staggered fermions have the advantage that they are fast to simulate and allow lattice QCD calculations with high statistics at relatively light quark masses, both requirements for accurate calculation of the masses of singlet pseudoscalar mesons.

However, lattice QCD calculations of the masses of the η and η' mesons face several challenges. The lattice QCD calculations of the flavour singlet mesons involve disconnected correlators which are computationally more expensive to compute than connected correlators. Also disconnected diagrams are inherently noisy in lattice simulations, so high statistics are required. The disconnected diagram for the pseudoscalar mesons is related to the topological charge of the gauge configuration which in some cases has been seen to have longer autocorrelation times than other quantities in lattice QCD simulations. To be sure statistical fluctuations and any autocorrelation times are well under control high statistics are required for an accurate lattice QCD calculation.

Although lattice QCD calculations that use improved staggered fermions have been suc-

cessfully tested against experiment for many quantities [13, 14], the formalism has not been proved to be fully correct because of the “fourth-root trick” employed to achieve the required flavour structure. There is increasing theoretical work [15, 16] that suggests that there are no problems with the improved staggered fermion formalism in the continuum limit, however the issue has not been completely settled. The $\eta\eta'$ system is a good place to check the validity of the rooting of the sea quark determinant, because of the important role the sea quark loops play in raising the mass of the η' meson. Creutz has recently claimed that the mass of the η' meson is a place where the improved staggered fermion formalism may not work [17, 18]. Kilcup and Venkataraman [9] have studied the flavour singlet pseudoscalar meson with naive staggered fermions in unquenched QCD.

The η and η' mesons can both be studied with lattice QCD calculations that include the dynamics of $2 + 1$ flavours of sea quarks. In a quark model treatment [19] of the η and η' mesons in terms of light and strange quarks:

$$\begin{aligned}\eta &\approx 0.58(\bar{u}\gamma_5 u + \bar{d}\gamma_5 d) - 0.57 \bar{s}\gamma_5 s \\ \eta' &\approx 0.40(\bar{u}\gamma_5 u + \bar{d}\gamma_5 d) + 0.82 \bar{s}\gamma_5 s .\end{aligned}$$

This suggests that both the η and η' mesons contain mixtures of light and strange quarks. The $\bar{u}u + \bar{d}d$ and $\bar{s}s$ interpolating operators will both couple to the η and η' mesons; in the singlet pseudoscalar channel the lightest state will be the η and the first excited state the η' meson. This is an additional complication of lattice QCD calculations that include $2+1$ flavours of sea quarks over those which only include 2 flavours of sea quarks. In $N_f = 2$ full lattice QCD calculations the emphasis is on finding the large mass splitting between the singlet pseudoscalar meson and the flavour non-singlet flavour mesons. With $2+1$ flavours of sea quarks it also interesting to see how the mass of the η meson is reproduced because this is sensitive to the mixing of $\bar{q}\gamma_5 q$ and $\bar{s}\gamma_5 s$ loops. The reader is referred to the review by Feldmann [20] for a recent discussion of $\eta\eta'$ mixing. The modern way to describe $\eta\eta'$ mixing is via leptonic decay constants [20]. See [4] for an attempt to compute the relevant decay constants in $N_f = 2$ unquenched QCD.

In this paper we report on the lattice methods required to study the singlet pseudoscalar mesons using improved staggered fermions. This work is the necessary starting point for a project that uses a large number of $N_f = 2 + 1$ configurations. For some cross-checks on the unquenched calculations we also study the singlet pseudoscalar meson in quenched QCD

and briefly investigate the role of topology.

The general plan of the paper is as follows: In Section II we describe the theory behind computing the correlators of singlet pseudoscalar mesons using improved staggered fermions. Next, in Section III, we describe the details of the calculation and report on the algorithmic work to compute the required disconnected diagrams. Section IV contains the results from the quenched and unquenched calculations and in Section V we discuss the statistics of singlet and non-singlet correlators. After that we estimate the number of configurations required to get a given accuracy in Section VI. The paper ends with our conclusions in Section VII.

II. THEORETICAL BACKGROUND

For notation, we use SP for the singlet pseudoscalar meson and NP for the non-singlet pseudoscalar meson. The additional complications due to staggered fermions are discussed later in this section. We begin with the expression of the pseudoscalar singlet propagator for N_f degenerate flavours of fermions:

$$G_{SP}(x', x) = \langle \sum_{i=1}^{N_f} \bar{q}_i(x') \gamma_5 q_i(x') \sum_{j=1}^{N_f} \bar{q}_j(x) \gamma_5 q_j(x) \rangle. \quad (1)$$

This propagator gives rise to two different types of diagrams. There are N_f connected diagrams:

$$\langle \sum_i \overbrace{\bar{q}_i(x') \gamma_5 q_i(x')} \underbrace{\sum_j \bar{q}_j(x) \gamma_5 q_j(x)} \rangle, \quad (2)$$

and N_f^2 disconnected terms:

$$\langle \sum_i \overbrace{\bar{q}_i(x') \gamma_5 q_i(x')} \sum_j \overbrace{\bar{q}_j(x) \gamma_5 q_j(x)} \rangle. \quad (3)$$

The connected term in the $N_f = 2$ flavour symmetric case is the same as that for the (non-singlet) pion propagator.

So we can write:

$$G_{SP}(x', x) = N_f C(x', x) - N_f^2 D(x', x), \quad (4)$$

where the extra fermion loop in the disconnected diagram gives rise to the relative minus sign, and

$$G_{NP}(x', x) = N_f C(x', x). \quad (5)$$

A. D/C ratio

In full Euclidean QCD we expect that the pion propagator should decay exponentially at large time separations as

$$G_{NP}(t) = Ae^{-m_{NP}t} \quad (6)$$

and similarly for the singlet propagator:

$$G_{SP}(t) = Be^{-m_{SP}t}. \quad (7)$$

As noted above the singlet propagator contains a disconnected and connected part, the latter being proportional to the pion propagator:

$$G_{SP}(t) = Ae^{-m_{NP}t} - N_f^2 D(t). \quad (8)$$

Taking the ratio $R(t)$ of the disconnected to connected parts at large time-separation Δt then suggests

$$R(t) = \frac{N_f^2 D(t)}{N_f C(t)} = 1 - \frac{B}{A} e^{-(m_{SP}-m_{NP})t}. \quad (9)$$

This derivation of (9) requires one to assume the same action is governing both sea quarks and valence quarks — in systems where the physics of the valence and sea quarks differ this expression may no longer apply. An important case of this is in the quenched limit where the D/C ratio is [9]

$$R(t) = A' + B't. \quad (10)$$

Another important case, relevant for staggered fermions, is when the number of flavours N_f of sea quarks differs from the native number of valence fermions, $N_v = 4$. In practice, this is the case for most staggered simulations — while the fourth-root trick reduces four degenerate sea flavours to the desired N_f , there remain four native valence flavours, or tastes, which contribute to singlet propagators. In the connected contribution (top diagram in Fig. 1) a single valence loop connecting the endpoints (meson interpolating operators) has four tastes of fermions circulating, introducing a factor of four. However in each of the terms of the disconnected contribution (bottom diagram in Fig. 1) there are two valence loops, one at each endpoint, each contributing a factor of four. The D/C ratio therefore naively has an extra factor of N_v and, if the staggered formulation (incorporating a fourth-root of the determinant) correctly reproduces N_f sea flavours, we expect:

$$R(t) = \frac{N_f^2 D(t)}{N_f C(t)} = N_v (1 - Ke^{-(m_{SP}-m_{NP})t}). \quad (11)$$

In the numerical work described in the following sections we implicitly rescale the disconnected contributions D by a factor of $1/4$ so as to correct for the extra valence tastes, a procedure which Sharpe calls “valence rooting” [15] and was used by Venkataraman and Kilcup in [9]. We will continue to refer to use the NP and SP notation, rather than introduce some new acronyms based on taste singlet notation.

There remains a possibility that the fourth-root trick could introduce some other pathologies at finite lattice spacing [17], e.g. the wrong number of sea flavours or a mismatch between sea and valence fermion masses [21]. Such issues should, in principle, be detectable in the D/C ratio.

For the case of N_f degenerate flavours there is only one possible interpolating operator for flavour singlet mesons for non-degenerate flavours of sea quarks there are more possible interpolating operators. In quark model inspired discussions of the $\eta\eta'$ mixing [19], the calculations use the $SU(3)$ octet η_8 and singlet η_0 basis states

$$\eta_0 = \frac{\bar{u}\gamma_5 u + \bar{d}\gamma_5 d + \bar{s}\gamma_5 s}{\sqrt{3}}$$

$$\eta_8 = \frac{\bar{u}\gamma_5 u + \bar{d}\gamma_5 d - 2\bar{s}\gamma_5 s}{\sqrt{6}}. \quad (12)$$

$$(13)$$

These basis states mix, because the $SU(3)$ symmetry is broken by the large mass of the strange quark, to form the physical η and η' mesons.

Another possible basis for flavour singlet pseudoscalar mesons is the quark basis, [20]

$$\eta_q = \frac{\bar{u}\gamma_5 u + \bar{d}\gamma_5 d}{\sqrt{2}}$$

$$\eta_s = \bar{s}\gamma_5 s. \quad (14)$$

The η_q and η_s will both also couple to the η and η' mesons, and are valid interpolating operators for flavour singlet pseudoscalar mesons. Each of these interpolating operators (η_q , η_s , η_0 and η_8) will have the η meson as the ground state and the η' as the first excited state.

In principle the 0^{-+} glueball could mix with the η and η' mesons. This would mean that a 0^{-+} glueball interpolating operator should also be used to study η and η' mesons. However quenched glueball simulations [22, 23] suggest the mass of the 0^{-+} glueball to be around 2.6 GeV. Since this is far from the mass of the η' , we do not consider the 0^{-+} glueball interpolating operator in what follows. Hart and Teper [24] studied the 0^{-+} glueball

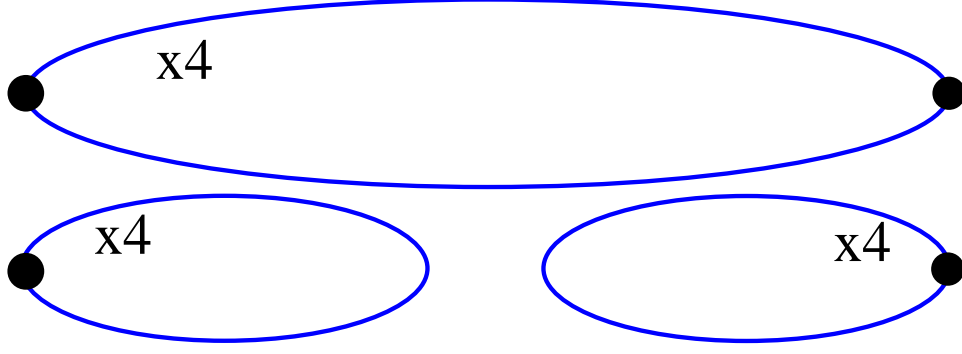


FIG. 1: The valence contribution to the connected (top) and disconnected (bottom) diagrams. There are natively $N_v = 4$ valence tastes in the staggered formulation, so each of these loops introduces a factor of four.

correlators in unquenched QCD and, despite large statistical errors, claimed the results were similar to those from quenched QCD.

The η does not decay via the strong interaction, hence the mass of the η is a gold-plated quantity [13] that should be possible to compute very accurately. The η' decays via the strong interaction but it has a small width of 0.2 MeV [25] (relative to that of the ρ meson, for example). The dominant strong interaction decay of the η' is via the decay to $\eta\pi\pi$ and thus we expect that this decay channel is not open for the masses we use. Thence we expect that an accurate calculation of the η' mass should be possible in principle.

For our $N_f = 2+1$ simulations, if we use the η_0 interpolating operator, we must generalise (4) and (9) to the case of non-degenerate flavours. The full propagator becomes

$$G_{SP\ SU3}(t) = 2C_{qq}(t) + C_{ss}(t) - 4D_{qq}(t) + 4D_{qs}(t) + D_{ss}(t), \quad (15)$$

and likewise the D/C ratio is

$$R(t)_{SU3} = \frac{4D_{qq}(t) + 4D_{qs}(t) + D_{ss}(t)}{2C_{qq}(t) + C_{ss}(t)}, \quad (16)$$

where D_{qq} , D_{qs} , and D_{ss} represent the disconnected correlators constructed with two light quark loops, one light and one strange quark loop, and two strange quark loops, respectively. Likewise C_{qq} and C_{ss} are the connected correlators measured with light and with strange quark masses, respectively.

B. Fitting the singlet propagator

With $2 + 1$ flavours of light quarks we have the potential to investigate the spectrum of both the η and the η' states. As discussed in Section I, in $2 + 1$ flavour calculations, the η' meson is the first excited state contributing to the pseudoscalar correlator. One approach would be to measure the appropriate connected and disconnected correlators, assemble the full singlet propagator in (15) and then fit to a multi-exponential form:

$$G(t)_{SP} = A_1 e^{-m_{SP1}t} + A_2 e^{-m_{SP2}t}. \quad (17)$$

However, fitting a multi-exponential expression with several parameters to data consisting of a single correlator can be difficult when that data is precise, and even more so when dealing with inherently noisy disconnected correlators.

In a multi-channel approach, treating the non-strange (q) and strange (s) contributions separately, using the quark basis (14) one would form the matrix

$$\begin{aligned} \mathbf{G}(\Delta t) &= \begin{bmatrix} \eta_q^\dagger(\Delta t)\eta_q(0) & \eta_q^\dagger(\Delta t)\eta_s(0) \\ \eta_s^\dagger(\Delta t)\eta_q(0) & \eta_s^\dagger(\Delta t)\eta_s(0) \end{bmatrix} \\ &= \begin{bmatrix} \mathbf{C}_{qq}(\Delta t) - 2\mathbf{D}_{qq}(\Delta t) & -\sqrt{2}\mathbf{D}_{qs}(\Delta t) \\ -\sqrt{2}\mathbf{D}_{sq}(\Delta t) & \mathbf{C}_{ss}(\Delta t) - \mathbf{D}_{ss}(\Delta t) \end{bmatrix}, \end{aligned} \quad (18)$$

and then fit

$$\mathbf{G}(t) = \mathbf{A}^T \mathbf{e}^{-\mathbf{m}t} \mathbf{A} \quad (19)$$

where \mathbf{A} is a matrix of amplitudes and $\mathbf{e}^{-\mathbf{m}t}$ is a diagonal matrix. This variational approach to fitting is one of the main methods of extracting masses and decay constants of excited mesons from lattice QCD calculations. The variational method is reviewed in [26] and used in [27, 28, 29, 30, 31]. The recent work on the η and η' mesons by the CP-PACS/JLQCD collaboration used the variational method [12].

Further improvement might be obtained by replacing the \mathbf{C} s and \mathbf{D} s in (18) by matrices of correlators formed with the various combinations of fuzzed and point source and sink operators. We leave investigation of such variational fits for future work.

N_f	$10/g^2$	$L^3 \times T$	am_{sea}	am_{val}	N_{cfg}
0	8.0	$16^3 \times 32$	—	0.020	76
2	7.2	$16^3 \times 32$	0.020	0.020	268
0	8.00	$20^3 \times 64$	—	0.020	408
0	8.00	$20^3 \times 64$	—	0.050	$408 \rightarrow 6154$
2	7.20	$20^3 \times 64$	0.020	0.020	547
2+1	6.76	$20^3 \times 64$	0.007, 0.05	0.007, 0.05	422
2+1	6.76	$20^3 \times 64$	0.010, 0.05	0.010, 0.05	644
2+1	6.85	$20^3 \times 64$	0.05, 0.05	0.05, 0.05	369

TABLE I: Ensembles used for singlet calculations.

Label	MILC	S0	S1	S2	S3	S4	S5	S6	S7	S8	S9	all
Configs	408	2455	413	414	409	411	409	410	409	412	412	6154

TABLE II: Quenched configurations in the MILC and extended ensemble streams.

III. SIMULATION AND MEASUREMENT

A. Configuration ensembles

We performed singlet correlator measurements on the $N_f = 0, 2$, and $2 + 1$ ensembles listed in Table I. We used $16^3 \times 32$ lattices for algorithm tuning as discussed below, and $20^3 \times 64$ lattices for physics measurements. The latter are primarily the so-called “coarse” lattice gauge configurations generated by the MILC collaboration [32] with the “Asqtad” improved staggered action [33, 34, 35, 36].

For analysis of the fluctuations in disconnected correlators (Section V) we extended the $\beta = 8.00$ quenched ensemble from 408 configurations to 6154 configurations. From the final configuration in the MILC ensemble, configuration 4090, we initiated ten separate Markov streams with 10 sweeps, each consisting of four over-relaxation steps and a quasi-heatbath hit, between saved configurations. These are listed in Table II.

B. Connected and disconnected correlators

The numerical calculation of the singlet propagator is performed in two parts — the calculation of the connected contributions, and the calculation of the disconnected contributions. The former is relatively straightforward — inversions on point source vectors produce quark propagators which are then multiplied together with an appropriate meson operator to produce a meson propagator.

There are in principle two different meson operators which couple to the flavour-singlet pseudoscalar meson. These are the $(\gamma_5 \otimes \mathbf{1})$ and the $(\gamma_4 \gamma_5 \otimes \mathbf{1})$, using the Kluberg-Stern [37] notation for the staggered meson operators. The former has the quark and anti-quark sources separated by four links, on opposite corners of the hypercube, while the latter has the quark and anti-quarks separated by three links, sited at opposite corners of the *spatial* cube. We write the operator as $(\gamma_5 \otimes \mathbf{1})$ to show that the meson has pseudoscalar Dirac structure, but is a singlet in Kogut-Susskind taste space.

As is generally the case with staggered meson operators, the operator which couples to the $(\gamma_4 \gamma_5 \otimes \mathbf{1})$ meson also couples to a parity partner state, which is in this case the $(\mathbf{1} \otimes \gamma_4 \gamma_5)$ scalar meson. The parity partner of the $(\gamma_5 \otimes \mathbf{1})$ however is exotic and therefore makes no contribution to the $(\gamma_5 \otimes \mathbf{1})$ propagator measured on the lattice. Furthermore, a variance reduction trick we discuss in Section III C applies only to the $(\gamma_5 \otimes \mathbf{1})$ operator. For these reasons we use the $(\gamma_5 \otimes \mathbf{1})$ state exclusively in this work.

To apply the $\Delta_{\gamma_5 \otimes \mathbf{1}}$ operator to a source vector or fermion propagator, we covariantly and symmetrically shift the source by one lattice unit in each of the four dimensions. We then apply the appropriate Kogut-Susskind phases [38], the exact formulation of this phase factor depending on the gamma-matrix conventions used in the simulation code.

Disconnected correlators are by nature noisy; they are directly sensitive to the fluctuations in the fermionic and gluonic sea. Consequently it is essential to extract more measurements from each configuration than can be gleaned from a single point source inversion. In order to achieve this we use the stochastic source method [39, 40, 41, 42]. A set of N_{src} independent noise source vectors $\{\eta^a\}$ ($a = 1, 2, \dots, N_{\text{src}}$) is chosen and normalised so that it has the orthogonality property

$$\langle \eta_i^{a\dagger} \eta_j^b \rangle_\eta = \delta_{ab} \delta_{ij} \quad (20)$$

where $\langle \rangle_\eta$ denotes the expectation value over all random noise η and i labels generically the

appropriate vector components such as space, Euclidean time, colour etc. Averaging over a sufficiently large number of samples N_{src} , the set of noise vectors then approximates the desired expectation value (20) and so reliable unbiased estimators for operators sums can be constructed. On a given configuration, and on each time slice t we calculate

$$\mathcal{O}_{\gamma_5 \otimes \mathbf{1}}(t) = \sum_{i \in t} \langle \eta_i^\dagger \Delta_{\gamma_5 \otimes \mathbf{1}} M_{ij}^{-1} \eta_j \rangle_\eta, \quad (21)$$

where the sum over i is restricted to the subset of lattice points on timeslice t and, from now on, $\langle \rangle_\eta$ denotes the expectation value estimated from the average over N_{src} noise vectors.

The Kentucky group has found analytically that among real noise sources, $Z(2)$ noise sources should offer the minimal variances for determining propagators [39]. We initially tested both complex $Z(2)$ and Gaussian noise sources on a small number of $16^3 \times 32$ $N_f = 2$ lattices and found that Gaussian noise sources produced slightly smaller errors than $Z(2)$ noise sources (see [43]). Based on this preliminary result we employed Gaussian volume sources for further simulation.

To investigate somewhat more thoroughly the apparent discrepancy between this and the Kentucky group's result we looked at a larger sample ($N_{\text{cfg}} = 67$) of $2 + 1$ -flavour $\beta = 6.76$ lattice configurations, and measured the light quark disconnected correlator $D_{qq}(\Delta t)$ using both $Z(2)$ and Gaussian noise source vectors. Since the size of the errors of disconnected correlators is found to be almost independent of the magnitude of the correlator itself, we averaged the error over the timeslice separation Δt allowing us to quote “errors on the errors”. In Fig. 2 the top two curves are the errors on the $\gamma_5 \otimes \mathbf{1}$ disconnected correlator measured with Gaussian noise (solid line) and with $Z(2)$ noise (dashed line) as a function of $1/N_{\text{src}}$. It is not apparent that either type of noise presents a large advantage over the other in the relevant region of $N_{\text{src}} \geq 8$.

These figures display the interesting property, previously noted in [44], that the errors of disconnected correlators measured with the volume noise source method appear to be inversely proportional to N_{src} , rather than to $\sqrt{N_{\text{src}}}$ as one might naively assume. In [45] Foley et al. attribute this to a property of the dilution method, however we find it to be a generic property of volume sources as well. This can best be understood by considering that while the loop operator on a given configuration (21)

$$\mathcal{O}_{\gamma_5 \otimes \mathbf{1}}(t) = \frac{1}{N_{\text{src}}} \sum_{a=1}^{N_{\text{src}}} \left[\sum_{i,j \in t} \eta_i^{a\dagger} \Delta_{\gamma_5 \otimes \mathbf{1}} M_{ij}^{-1} \eta_j^a \right], \quad (22)$$

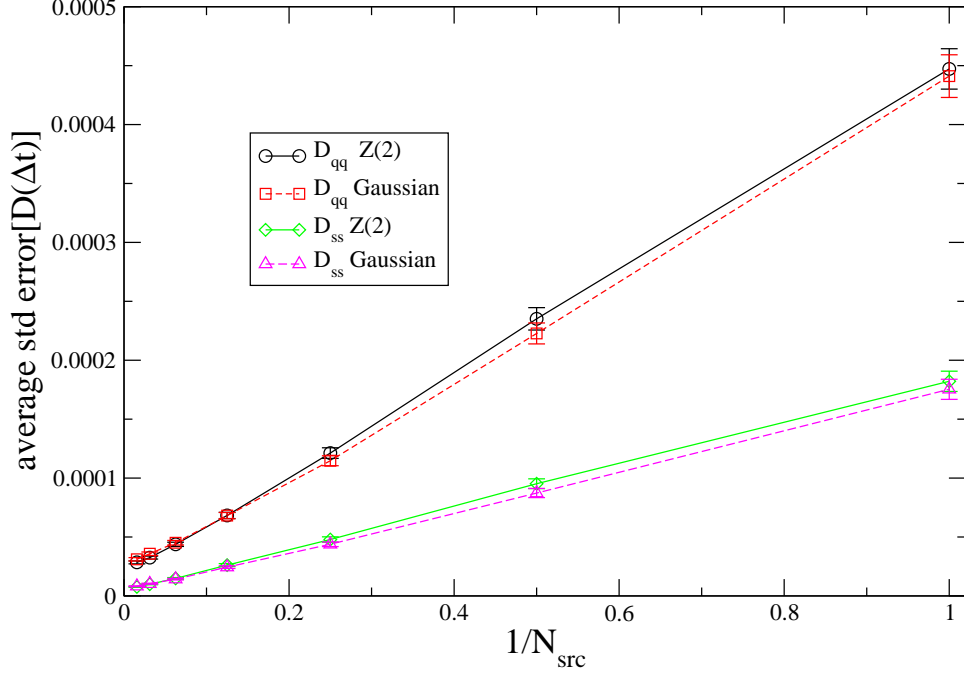


FIG. 2: A comparison of Gaussian and $Z(2)$ noise sources for $67 \times 20^3 \times 64$ $N_f = 2 + 1$ lattices for $\beta = 6.76$ $am = 0.01, 0.05$. The plot shows the standard error on the disconnected correlator $D(\Delta t)$, averaged over Δt , versus inverse number of noise sources for the standard $(\gamma_5 \otimes \mathbf{1})$ operator.

has N_{src} terms in the sum over noise sources, the disconnected correlator on that configuration has N_{src}^2 terms:

$$\begin{aligned} \mathcal{D}_{\gamma_5 \otimes \mathbf{1}}(\Delta t) &= \mathcal{O}_{\gamma_5 \otimes \mathbf{1}}(t) \mathcal{O}_{\gamma_5 \otimes \mathbf{1}}(t + \Delta t) \\ &= \frac{1}{N_{\text{src}}^2} \sum_{a=1}^{N_{\text{src}}} \sum_{b=1}^{N_{\text{src}}} \left[\sum_{i,j \in t} \eta_i^{a\dagger} \Delta_{\gamma_5 \otimes \mathbf{1}} M_{ij}^{-1} \eta_j^a \right] \left[\sum_{k,l \in t+\Delta t} \eta_k^{b\dagger} \Delta_{\gamma_5 \otimes \mathbf{1}} M_{kl}^{-1} \eta_l^b \right], \end{aligned} \quad (23)$$

so the variance likewise decreases like $1/N_{\text{src}}^2$.

C. Variance reduction

Results from the TrinLat collaboration, using Wilson like fermions, indicate that variance is reduced by using “diluted” noise sources when using stochastic sources to measure connected correlators [45]. As the name implies, such diluted sources are non-zero only on some subset of the lattice. It is then important to use a set of sources for which the non-zero subsets together span the entire lattice volume. The subsets may, for example, be time-slices, colors, or hypercube corners. We tested several noise dilution schemes in the present

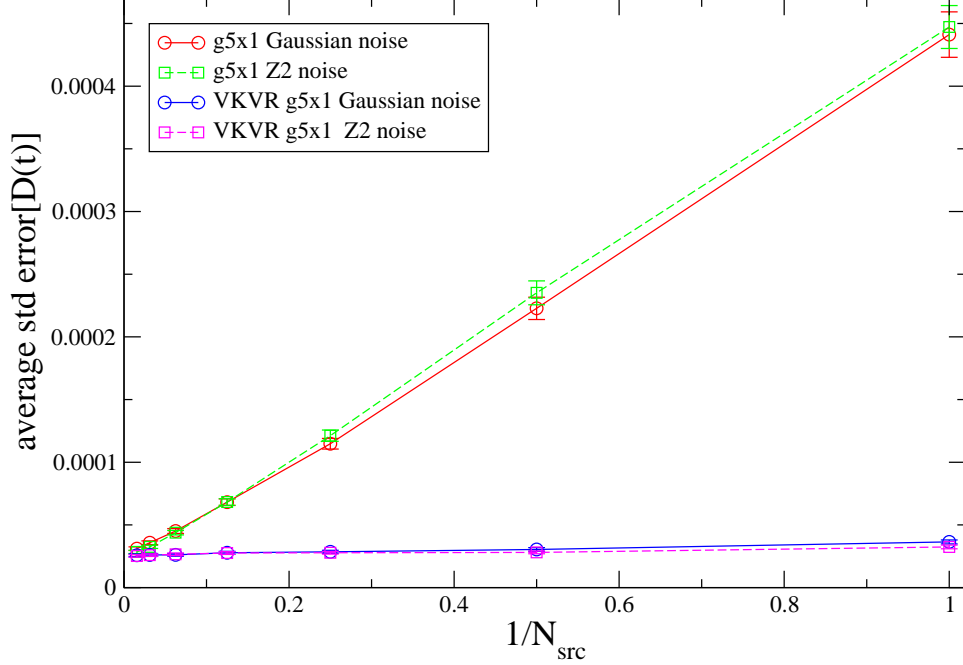


FIG. 3: The dependence of the error on $D_{qq}(t)$ with $1/N_{\text{src}}$ for the 67 lattice configurations described in Fig. 2. The comparison is for $Z(2)$ and Gaussian noise for both standard and VKVR-improved $(\gamma_5 \otimes \mathbf{1})$ operators (see text).

application and found no advantage over using traditional volume-filling sources (see [46]).

In [9], Venkataraman and Kilcup introduce a variance reduction technique that is applicable for the the $(\gamma_5 \otimes \mathbf{1})$ staggered meson operator. The Venkataraman-Kilcup variance reduction (VKVR) trick uses the fact that the staggered Dirac operator $M = (\not{D} + m)$ and its Asqtad-improved variants (and their inverses) connect sites separated by an odd number of links. Likewise $M^\dagger M$ and its inverse connect sites separated by an even number of gauge links. Here we recall that the quark and anti-quark are displaced from each other by four links by the $(\gamma_5 \otimes \mathbf{1})$ operator. Now

$$\eta_x M^{-1} \eta_y$$

is clearly

$$\eta_x (M^\dagger M)^{-1} M^\dagger \eta_y = \eta_x (M^\dagger M)^{-1} (-\not{D} + m) \eta_y. \quad (24)$$

However, since the sites denoted by x and y (quark and antiquark) are 4 links apart, the term proportional to \not{D} has zero expectation value so

$$\langle \eta_x M^{-1} \eta_y \rangle_\eta = m \langle \eta_x (M^\dagger M)^{-1} \eta_y \rangle_\eta. \quad (25)$$

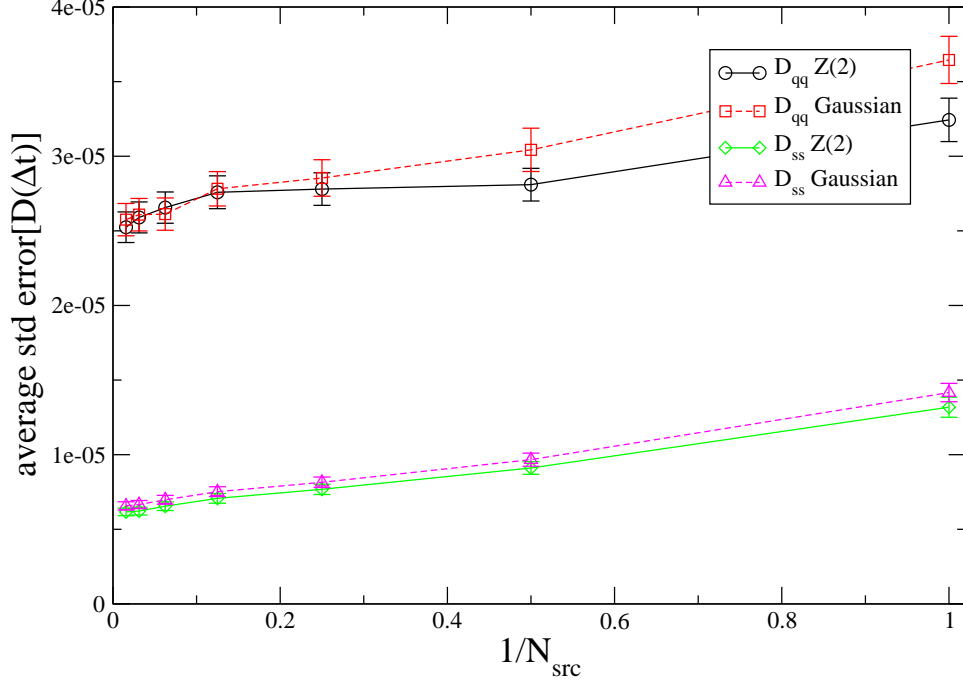


FIG. 4: Dependence of the averaged standard error of $D_{qq}(t)$ and $D_{ss}(t)$ on $1/N_{\text{src}}$ for the 67 lattice configurations described in Fig.. 2. VKVR-improved ($\gamma_5 \otimes \mathbf{1}$) operators are used.

It turns out, however, that the right-hand expression has a significantly decreased variance with respect to stochastic noise. There is no additional computational cost since we are already computing $\phi = M^{-1}\eta$, and we can express the right hand side of (25) as $m\langle\phi^\dagger\phi\rangle$.

As the VKVR trick should be applicable to disconnected loops for any meson operator with the quark and antiquark separated by an even number of lattice spacings, for example the $(\mathbf{1} \otimes \mathbf{1})$ scalar meson.

The error on elements of the disconnected correlators is composed of a stochastic part — which decreases like $1/N_{\text{src}}$ as mentioned above — and a gauge part, which remains after $N_{\text{src}} \rightarrow \infty$ and decreases as $1/\sqrt{N_{\text{cfg}}}$. The effect of the VKVR trick on disconnected correlator errors is dramatic. Fig. 3 shows the error on the disconnected correlator (averaged over time separations) as a function of the inverse number of noise sources. With just a few noise sources the VKVR trick nearly eliminates all of the stochastic component of the error on D_{qq} . At $N_{\text{src}} = 64$ the magnitude of the errors on the VKVR and normal $\gamma_5 \otimes \mathbf{1}$ disconnected correlators become comparable (Fig. 3 and Fig. 5).

To calculate the connected and disconnected correlators of the $\gamma_5 \otimes \mathbf{1}$ state we wrote specialised routines for the Chroma software system [47].

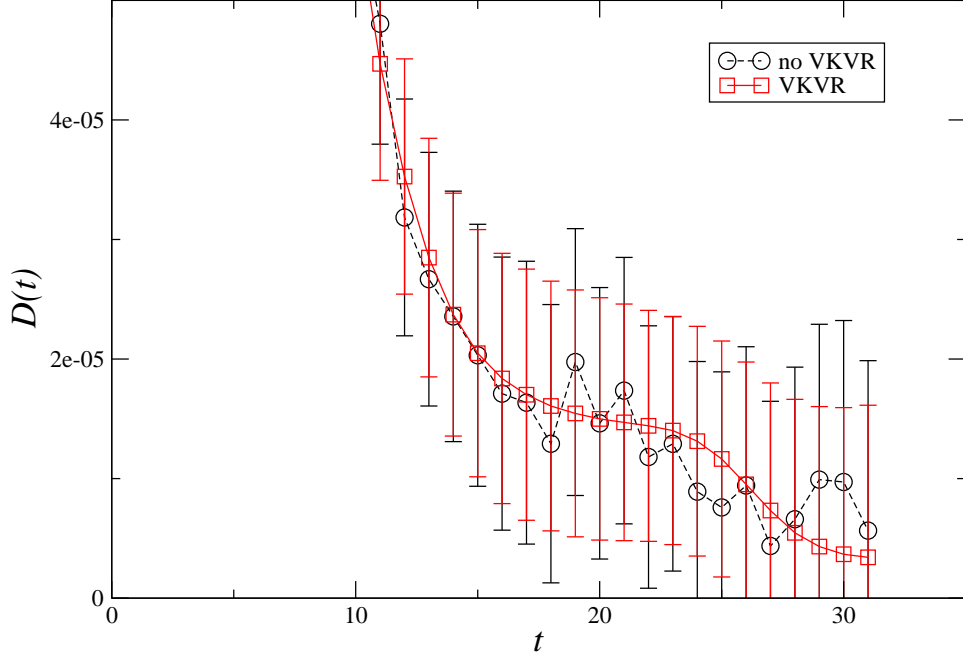


FIG. 5: A comparison of disconnected correlators for $\beta = 6.76$ $am = 0.01$ obtained with and without using the VKVR variance reduced operators for $N_{\text{src}} = 64$.

On each configuration, for the light and strange quark masses, we calculated the connected correlator for the singlet pion ($\gamma_5 \otimes \mathbf{1}$). We also calculated the mean of $\text{Tr} [\Delta_{\gamma_5 \otimes \mathbf{1}} M^{-1}]$ on each timeslice using $N_{\text{src}} = 64$ Gaussian noise sources for each. The latter we use to calculate disconnected correlators. We then use all of these quantities to make the D/C ratio as in Equation 16. We fit $R(t)$ to the functional form in (9) to determine the splitting between the pion and singlet masses.

IV. RESULTS

A. Quenched analysis

With the availability of improved algorithms and significantly more powerful computational resources, the quenched approximation to lattice QCD no longer plays such a significant role. However, it remains instructive to study singlet pseudoscalar mesons from quenched lattice QCD calculations. In particular the Witten-Veneziano relation relates the topological susceptibility, in the large N limit of the $SU(N)$ pure gauge theory, to a contribution to the mass of the η' meson. A comparison between quenched and full-QCD systems

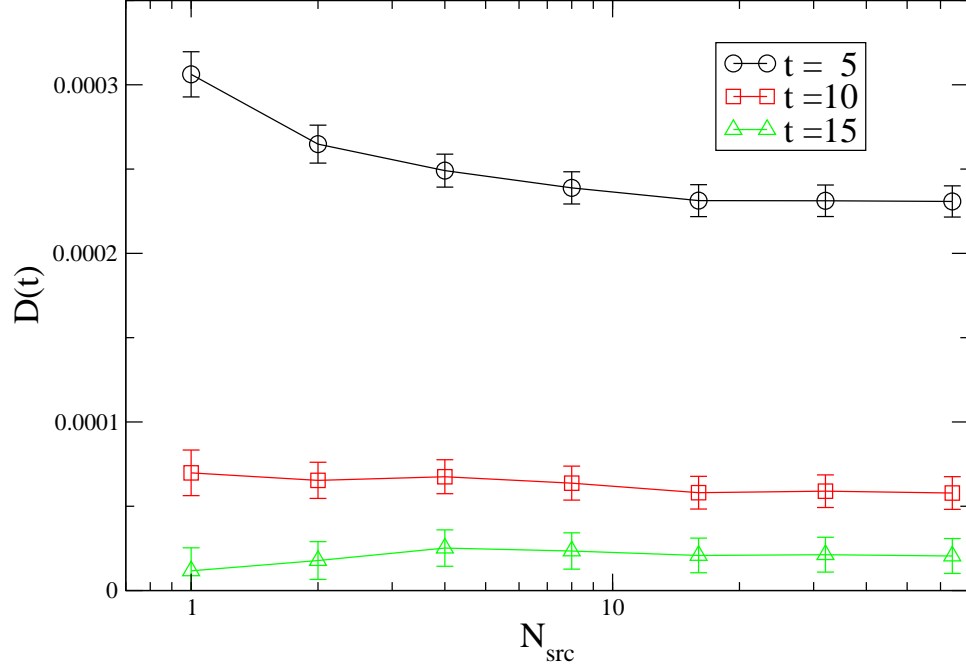


FIG. 6: Dependence of $D_{qq}(t)$ on N_{src} for 658 $\beta = 6.76$ $am = 0.01$ $20^3 \times 64$ lattices.

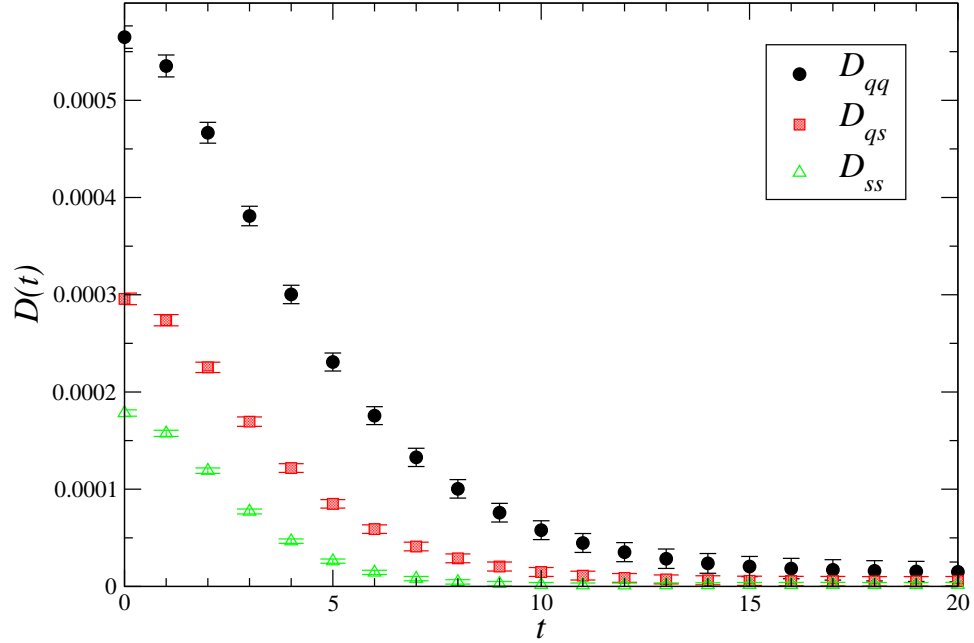


FIG. 7: Disconnected correlators for 658 $\beta = 6.76$ $am = 0.01$ $20^3 \times 64$ lattices.

highlights the effect of dynamical sea quarks. This is particularly instructive in studying flavour singlet mesons. Further, since quenched configurations are cheap to generate, one can use very large ensembles to illuminate the nature of the statistical fluctuations of singlet

quantities and possible long auto-correlation times associated with slow topological modes.

We calculated connected and disconnected correlators on the quenched gauge configurations at $\beta = 8.00$ (neglecting 8 thermalisation configurations) with a valence mass of 0.05. In Figure 8 the ratio $R(t)$ is plotted for all the quenched configurations, as well as for subsets of the quenched configurations. Quenched staggered QCD involves no determinant fourth-roots so there are no obvious theoretical reasons for a significant deviation from (10) for the MILC ensemble, when lattice artifacts and finite size effects are neglected. The original MILC coarse quenched ensemble ($\beta = 8.00$) had 408 configurations, and upon extending the quenched ensemble as described in Section III and Table II, we see from Fig. 8 that the D/C ratio calculated with the full 6154 configurations is more linear and, as such, in better agreement with the expression (10) for $\Delta t \leq 15$.

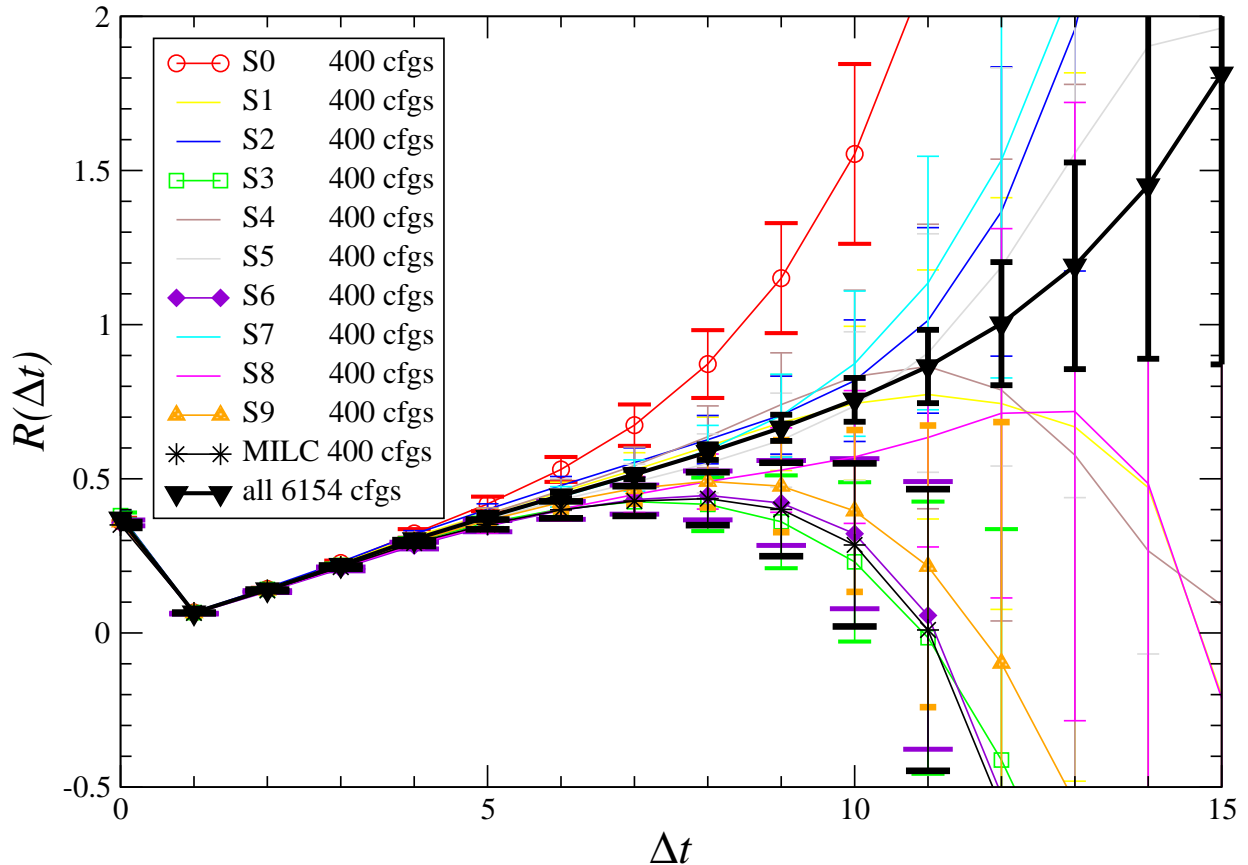


FIG. 8: D/C ratio for 6154 $\beta = 8.00$ quenched lattices with valence quark mass $am = 0.05$, and for 11 subsets of 400 configurations. We highlight five of these subsets, including the original MILC configurations, as disagreeing with the mean by more than one σ .

In Fig. 9 we show the effective mass plots for the light $\gamma_5 \otimes \mathbf{1}$ and $\gamma_5 \otimes \gamma_5$ non-singlet

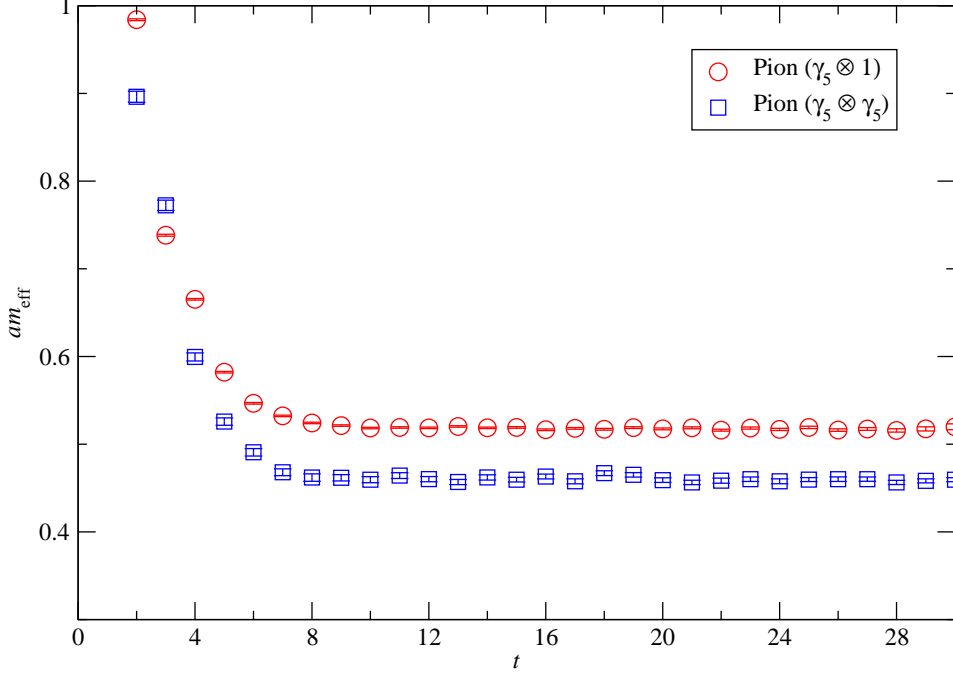


FIG. 9: Effective masses for the $\gamma_5 \otimes \gamma_5$ and $\gamma_5 \otimes \mathbf{1}$ pseudoscalar mesons for the quenched data set ($\beta = 8.0$).

pseudoscalar mesons. We computed correlators for the $\gamma_5 \otimes \gamma_5$ pseudoscalar mesons only on the original data set, but computed the $\gamma_5 \otimes \mathbf{1}$ connected and disconnected correlators on the full extended data set.

In Table III we report the masses for the $\gamma_5 \otimes \mathbf{1}$ and $\gamma_5 \otimes \gamma_5$ pseudoscalar mesons. The fits included the full correlation matrix in time and we report both one- and two-cosh mass fits. The MILC collaboration obtained the mass 0.46043(20) for the mass of the $\gamma_5 \otimes \gamma_5$ pseudoscalar meson, using Coulomb gauge fixed wall sources [32]. This is in good agreement with our value in Table III. As expected, the inclusion of the second state allows us to fit much closer to the origin [14].

Quenched chiral perturbation theory [9, 48] makes predictions for the ratio of disconnected and connected correlators:

$$R(t) = \frac{(m_0^2 - \alpha m_{NP}^2)}{2m_{NP}}t + \frac{m_0^2 + \alpha m_{NP}^2}{2m_{NP}^2} \quad (26)$$

where α is the parameter of the kinetic term of singlet pseudoscalar meson [48], and m_0 is the difference between the masses m_{SP} and m_{NP} . Comparing (26) with (10) we see that it defines the parameters A' and B' in (10).

TABLE III: Masses for the light pseudoscalars mesons (using connected correlators only) from the quenched data set ($\beta = 8.00$). The $\gamma_5 \otimes \mathbf{1}$ correlators were measured with 8 times the statistics of the $\gamma_5 \otimes \gamma_5$ channel.

Channel	t-region	am_1	am_2	χ^2/dof
$\gamma_5 \otimes \gamma_5$	13-26	0.4601(6)	-	16.8/ 12
$\gamma_5 \otimes \gamma_5$	5-25	0.4603(6)	1.88(56)	23.1/17
$\gamma_5 \otimes \mathbf{1}$	11-24	0.5182(3)	-	14.2 / 12
$\gamma_5 \otimes \mathbf{1}$	5-23	0.5180(3)	1.27(5)	17.1/16

The value of α is expected to be small, so we neglect it [9, 48] — indeed Bardeen et al. [49] estimate that $\alpha = 0.03 \pm 0.03$ and advocate setting $\alpha = 0$.

Fitting the quenched $D(t)/C(t)$ data to the model in (10), we obtain a slope of $B' = 0.068(3)$. Using the mass of the $\gamma_5 \otimes \mathbf{1}$ pseudoscalar meson from Table III and $B' = \frac{m_0^2}{2m_{NP}^2}$, we obtain $m_0 = 0.76(2)$ GeV, where we have multiplied by $\sqrt{n_f} = \sqrt{3}$ [50].

In Fig. 10 our value for m_0 and the values from Bardeen et al. [49, 51] are plotted against the square of the pion mass in units of r_0 . The results from Bardeen et al. [49, 51] at $\beta = 5.9$ were used with the value of r_0/a from the ALPHA collaboration [52].

Estimates for the value of m_0 , in the chiral limit, can also be obtained from the Witten-Veneziano relation

$$m_0^2 = \frac{4N_f \chi_T}{f_\pi^2} \quad (27)$$

where the topological susceptibility χ_T is evaluated in the large N_c limit of the pure gauge theory and using f_π with a normalisation of 132 MeV. Shore [53] describes a modern approach to the use of the topological susceptibility in the study of η and η' mesons. Lucini and Teper [54] have shown that the topological susceptibility is only weakly dependent on the number of colours.

The MILC collaboration [55] obtained $\chi_T r_0^4 = 0.0543(28)$ at $\beta = 8.00$, and $\chi_T r_0^4 = 0.0569(26)$ at $\beta = 8.40$. These numbers are in good agreement with other quenched results such as those by Del Debbio et al. [56], who obtain $\chi_T r_0^4 = 0.059(3)$ in the continuum limit. There has also been a recent calculation by Durr et al. [57], who obtain $\chi_T r_0^4 = 0.0524(7)(6)$ in the continuum limit.

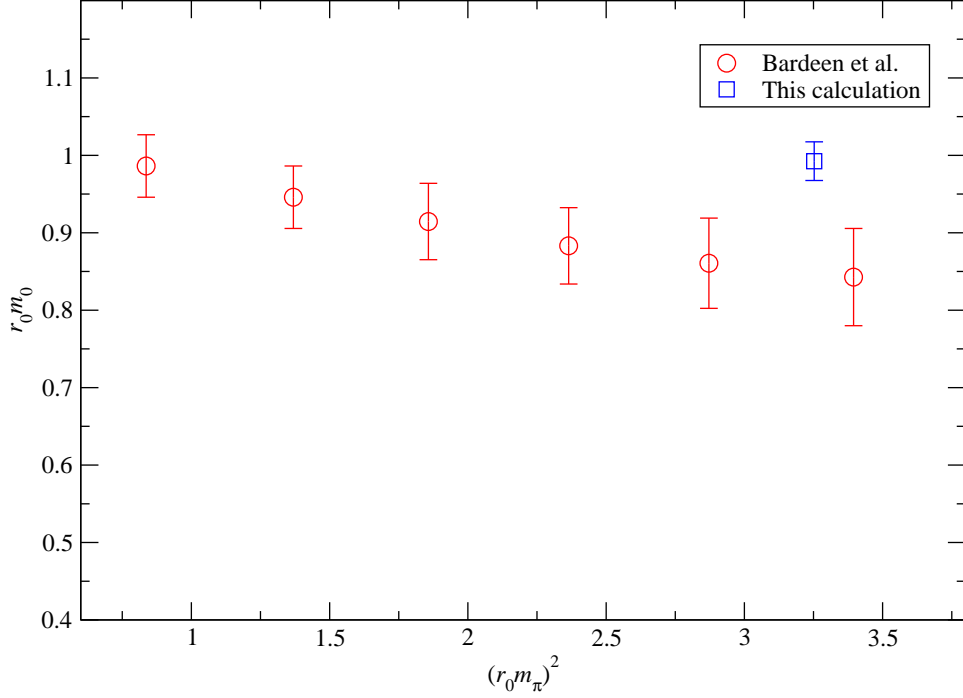


FIG. 10: Mass dependence of the m_0 from Bardeen et al. [49] and this calculation in units of r_0 . There are no factors of n_f included.

Using $\chi_T r_0^4 = 0.0543(28)$ in (27) with $N_f = 3$, and taking the value of $r_0 = 0.467$ fm from the HPQCD and MILC collaborations, one obtains $m_0^2 = (1.09 \text{ GeV})^2$. Using the value of $r_0 = 0.5$ fm, instead, one would obtain $m_0^2 = (.952 \text{ GeV})^2$.

The value of m_0 can also be estimated from [19], assuming that the η is a pure SU(3) octet and the η' is the SU(3) singlet.

$$m_0^2 = m_{\eta'}^2 + m_\eta^2 - 2m_K^2 \quad (28)$$

This method gives a value of $m_0^2 = (0.854 \text{ MeV})^2$.

The mass dependence of the m_0 parameter has recently been discussed by Sharpe [58]. In quenched lattice calculations, Kuramashi et al. [50] found that the m_0 parameter had a negative slope with respect to the quark mass where it is more usual to see a positive slope (see the results by MILC [14]). Sharpe's predictions were tested by Bardeen et al. [51]. Liu and Lagae [59] found that a novel mass-dependent renormalisation factor removed the bulk of the mass dependence of m_0 observed in the study by Kuramashi et al. [50].

Our result $m_0 = 0.76(2) \text{ GeV}$ described above, with the valence quark mass set approxi-

mately to that of the strange quark, is consistent with other estimates. A chiral extrapolation would be required to make a more precise comparison.

B. Unquenched analysis

In Fig. 11 we present effective mass plots for the $(\gamma_5 \otimes \mathbf{1})$ correlators, with the connected and sum of connected and disconnected correlators, for the $\beta=6.76$, $m_q/m_s = 0.01/0.05$ data set. The effective mass from a correlator of a disconnected loop at the light quark mass with a disconnected loop at the strange quark mass is also included in Fig. 11.

In Table IV we report single- and double-exponential fits to the connected $\gamma_5 \otimes \mathbf{1}$ pseudoscalar correlators. MILC obtained the masses of the $\gamma_5 \otimes \gamma_5$ pseudoscalar mesons to be $0.22446(22)$ and $0.49443(25)$ in lattice units for the light and strange quarks respectively [32]. At this lattice spacing the light $\gamma_5 \otimes \mathbf{1}$ pseudoscalar meson is split from the $\gamma_5 \otimes \gamma_5$ pseudoscalar meson by about 200 MeV. This mass splitting is caused by taste violations and is expected to go to zero as the continuum limit is taken. Indeed, the MILC collaboration has presented evidence that the mass splittings between different pseudoscalar mesons go like $O(\alpha_s^2 a^2)$, as expected, for this action [14].

If the mass splitting between the connected $\gamma_5 \otimes \mathbf{1}$ pseudoscalar mesons and the $\gamma_5 \otimes \gamma_5$ correlator was taken as a systematic error at this lattice spacing, then this would imply the error in the η mass at this lattice spacing is roughly 30%.

In the twisted mass formalism there is a flavour symmetry breaking term that causes a mass splitting between the π^0 and π^+ mesons at non-zero lattice spacing. Although the physics of flavour symmetry breaking is different for staggered fermions [36] and the twisted formalism, it is encouraging that experience with the twisted mass formalism has shown that the disconnected diagrams reduce the mass splitting between the masses of the π^0 and π^+ mesons, caused by isospin violation outside the continuum limit, over the estimate from the connected correlators [60].

We see from Table V that consistent ground states are determined from the $\bar{s}\gamma_5 s$ and $\bar{q}\gamma_5 q$ operators when the disconnected diagrams are included. This is non-trivial, particularly because the masses from the connected correlators are very different for light and strange quarks. This is true because the physical η contains both $\bar{s}\gamma_5 s$ and $\bar{q}\gamma_5 q$ quark content, so either interpolating operator should couple to the η meson and produce the

same ground state mass. The $\eta - \eta'$ mixing is further discussed in Section II. The recent CP-PACS/JLQCD calculations enforced a consistent mass for the $\bar{s}s$ and $\bar{q}q$ operators using their variational method [12]. The contribution from the disconnected part of the correlators appears to compensate for the increase of the masses from the connected part.

The correlator between a light and strange pseudoscalar loop should also couple to the η and η' mesons. Fig. 11 shows that the correlator between a light quark loop and strange quark loop (off-diagonal part of (18)) seems to have a plateau at a mass different to the value from light or strange correlators (diagonal parts of (18)). It is not clear why this happening — Aubin and Bernard have published propagators for the neutral η from staggered chiral perturbation theory [61], but unfortunately these do not include terms for $\eta - \eta'$ mixing that are essential for this analysis. One obvious possibility is that the ground state is not being isolated for the singlet correlators in Fig. 11. It has been noted before by the SESAM collaboration and Bardeen et al. [49, 51] that the majority of the excited state contamination in a flavour singlet pseudoscalar correlator is from the connected part of the correlator. Hence the correlator of a strange loop with a light quark loop could approach the ground state at a different rate to correlators with a connected contribution. Given that the signal for correlators that include a disconnected contribution in Fig. 11 dies in the noise beyond timeslice 7, it is difficult to tell where the true plateau lies.

We tried the variational analysis discussed in Section II B. The χ^2/dof of the fits were larger than 7. The problem is, as we discussed above, that the correlators for a light loop to strange loop seem to be plateauing at different mass to the singlet light and strange loops. The variational fitting formula (19) assumes that each element of the smearing matrix couples to the same ground state. We also tried looking at eigenvalues of the matrix, but the two eigenvalues just reproduced the diagonal and off diagonal correlators. One possibility would be that there is a normalisation problem between the disconnected and connected loops. However the magnitude of the light disconnected loop is much larger than that of the strange disconnected loop, so a consistent change in the normalisation of the disconnected loops makes it hard to get the effective mass of the light-light correlator to plateau at the same mass as the strange-strange correlator. This is also a prerequisite for the variational analysis.

The analysis of the non-singlet a_0 correlator using improved staggered fermions turned out to be possible, but non-trivial [62, 63]. In this case the ground state for the singlet

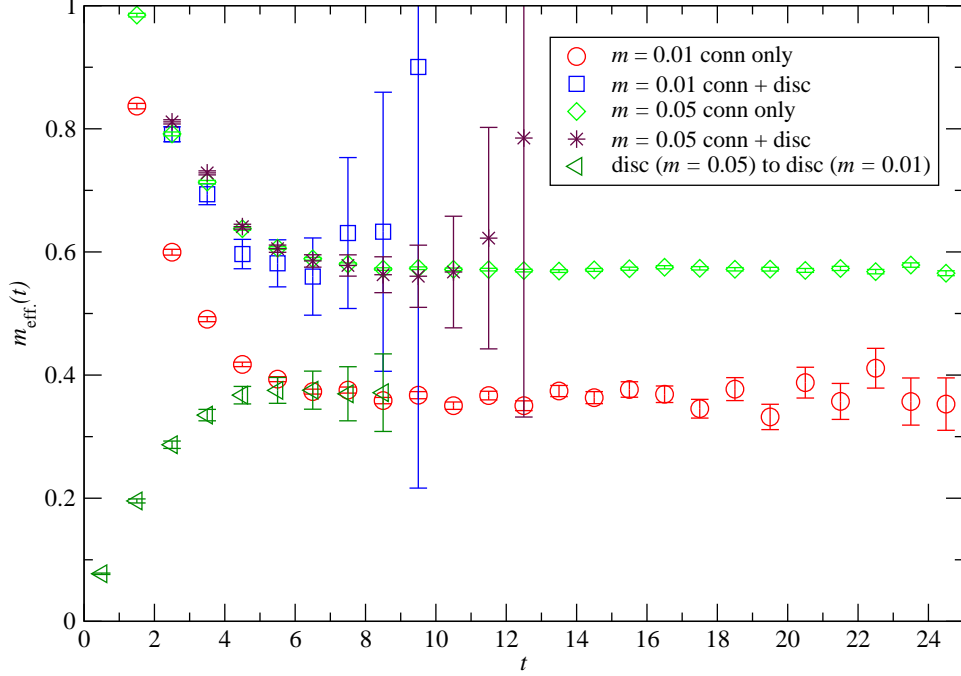


FIG. 11: Effective masses for the $(\gamma_5 \otimes \mathbf{1})$ channel for the light and strange quarks for the $\beta = 6.76$, $m=0.01/0.05$ data set.

pseudoscalar channel is the η that is stable under the strong interactions.

The numbers for the lightest mass in Table V are about 0.6 in lattice units with weak quark mass dependence. This corresponds to a mass in physical units of 990 MeV — the ground state in this channel should be the η with a mass of 548 MeV. The masses in Table V are probably contaminated by excited state contributions, so are only an upper limit. A fit to the mixed disconnected correlator of a light quark disconnected loop at $am_q = 0.01$ with a strange quark disconnected loop at mass $am_s = 0.05$ in Fig. 11 gives a mass around 600 MeV. Unfortunately because this number does not agree with that from the diagonal correlators we do not use it to quote a physical mass for the lightest flavour singlet pseudoscalar meson.

Fig. 12 shows the ratios of disconnected to connected correlators as defined by (16) in the non-degenerate unquenched case (the quenched data is also shown for comparison). The ratio plots show that the errors get very large as t gets large. This makes the test that the $D(t)/C(t)$ tends to 1 in the large Δt limit difficult to judge from looking at the graphs. With the unquenched data we constructed both $R(t)_{SU3}$ (defined by (16)), and the single-flavour

TABLE IV: Masses for the light pseudoscalars mesons for the unquenched data sets obtained from $(\gamma_5 \otimes \mathbf{1})$ connected correlators.

β	m_l/m_s	m_v	region	am_1	am_2	χ^2/dof
6.76	0.01/0.05	0.05	10-17	0.572(1)	-	5.5/6
6.76	0.01/0.05	0.05	5-11	0.571(2)	1.27(11)	3.5/3
6.76	0.007/0.05	0.05	11-16	0.566(2)	-	2.6/4
6.76	0.007/0.05	0.05	5-11	0.567(3)	1.19(13)	4.6/3
6.76	0.01/0.05	0.01	11-16	0.363(4)	-	4.8/4
6.76	0.01/0.05	0.01	4-11	0.358(5)	1.00(12)	4.3/4
6.76	0.007/0.05	0.007	11-16	0.331(6)	-	0.6/4
6.76	0.007/0.05	0.007	5-11	0.33(1)	0.91(34)	2.9/3
6.85	0.05/0.05	0.05	12-17	0.553(2)	-	3.8/4
6.85	0.05/0.05	0.05	4-14	0.554(2)	1.33(8)	8.7/7

TABLE V: Masses for the light $(\gamma_5 \otimes \mathbf{1})$ pseudoscalars mesons for the unquenched data sets, from the correlators that includes the disconnected diagram.

β	m_q/m_s	m_v	region	am_1	χ^2/dof
6.85	0.05/0.05	0.05	7-11	0.64(16)	1.6/3
6.76	0.01/0.05	0.05	5-11	0.59(2)	0.4/3
6.76	0.007/0.05	0.05	5-9	0.59(2)	1.4/4
6.76	0.01/0.05	0.01	4-9	0.58(6)	0.6/3
6.76	0.007/0.05	0.007	5-9	0.64(9)	1.4/3

$R(t) = D(t)/C(t)$ and fitted both to the model

$$R(t) = A_0 + B_0 e^{-(m_r t)}, \quad (29)$$

where m_r is the mass difference between the taste singlet pseudoscalar meson and the connected pseudoscalar correlator. The results for the three fit parameters are given in Table VI. In the table we compare m_r , obtained from the ratio, to am_r^{diff} . We define the latter to be

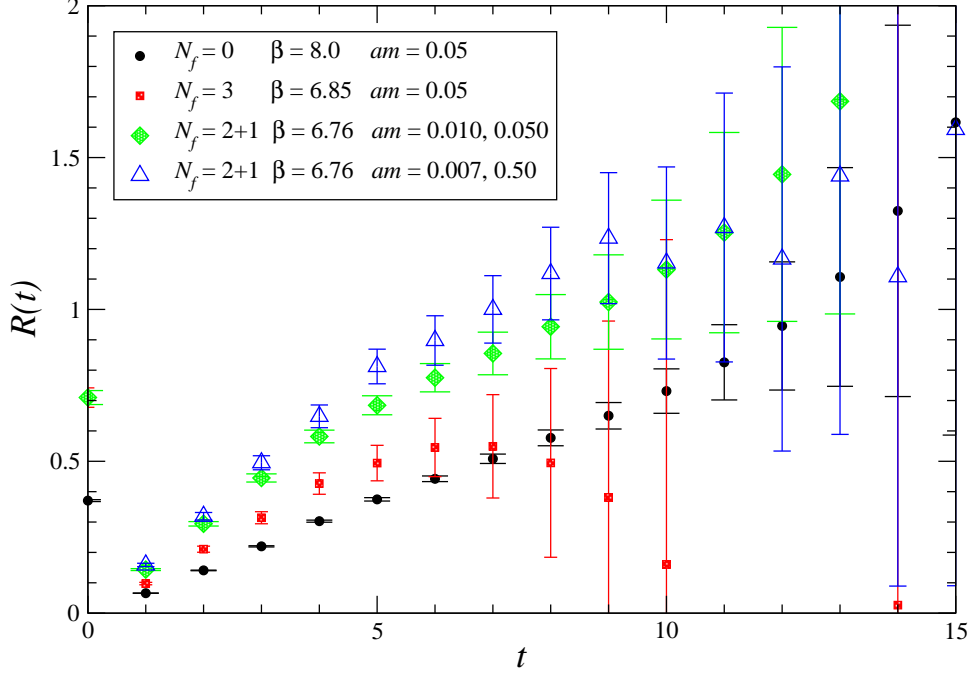


FIG. 12: D/C ratio for coarse MILC ensembles. For the $N_f = 3$ and $N_f = 2 + 1$ ensembles R_{SU3} is displayed. For the quenched configurations the single-flavour $R = D/C$ is plotted.

the mass of the taste singlet pseudoscalar meson, obtained from the matrix propagator (18) and listed in Table V, with the mass from the pure connected state (Table IV) subtracted off.

Within the large 30% errors A_0 is 1 for the light quark as expected from theory. Also the values of $am_{\nu_r}^{\text{diff}}$ are consistent with am_r . Given the noise in the calculation the starting times in the fit could only be moved 1 or 2 time units forwards or backwards from those quoted in Table VI, so a more convincing test would require much higher statistics. Unfortunately we were unable to get stable fits of the D/C ratio for the $N_f = 3$ $\beta = 6.85$ data set, probably because the statistics at $\beta = 6.85$ were lower than for the other β values.

C. Topological Charge

Smit and Vink [64] have pointed out that from the Atiyah-Singer index theorem [65] it follows that the $\gamma_5 \otimes \mathbf{1}$ quark loop is a measure of the topological charge density. Having measured this quantity as part of the disconnected correlator calculation we are in a position

TABLE VI: Parameters from the fit of (29) to the unquenched data. The result for m_r^{diff} is from the difference between the mass of the taste singlet and the connected pseudoscalar channel. The SU3 entry corresponds to the use of the R ratio in eq. 15.

β	m_q/m_s	Mass	region	A_0	B_0	am_r	am_r^{diff}	χ^2/dof
6.76	0.01/0.05	0.01	5 - 13	1.03(35)	-0.97(23)	0.15(11)	0.22(6)	6.1/6
6.76	0.01/0.05	SU3	4 - 11	1.01(19)	-1.15(9)	0.24(9)	0.22(6)	6.3/5
6.76	0.007/0.05	0.007	4 - 9	1.14(39)	-1.47(23)	0.24(18)	0.31(9)	1.5/3
6.76	0.007/0.05	SU3	4 - 8	1.15(30)	-2.09(91)	0.35(24)	0.31(9)	1.2/2

to compare the fermionic definition of topological charge

$$Q = m\kappa_p \langle \text{Tr} (\gamma_5 M^{-1}) \rangle_U, \quad (30)$$

where κ_p is a renormalisation factor, with the traditional gluonic definition

$$Q = \frac{g^2}{64\pi^2} \int dx \epsilon^{\mu\nu\rho\sigma} F_{\mu\nu}^a(x) F_{\rho\sigma}^a(x). \quad (31)$$

Alles *et al.* have performed a similar comparison with Wilson fermions [66]. The MILC collaboration has extensively studied the topology on these lattices using gluonic definitions of the topological charge [55, 67].

We used the publicly available MILC code [68] to measure the topological charge. The gauge fields were cooled by hypercubic blocking [55, 69, 70] before the topological charge was measured.

A comparison of the two definitions of topological charge on 198 $N_f = 2 + 1$, $\beta = 6.76$ lattices is shown in Fig. 13, and shows that the gluonic definition of the topological charge is strongly correlated with the fermionic definition. This gives us confidence that the staggered $\langle \text{Tr} (\gamma_5 M^{-1}) \rangle$ operator, which is a key building block in the SP correlator, is behaving as expected. A more empirical comparison between the fermionic and gluonic topological charge requires knowledge of the renormalisation factors. Methods have been developed [57, 71] to determine the matching renormalisation factor between the two definitions of the topological charge, based on their assumed equality.

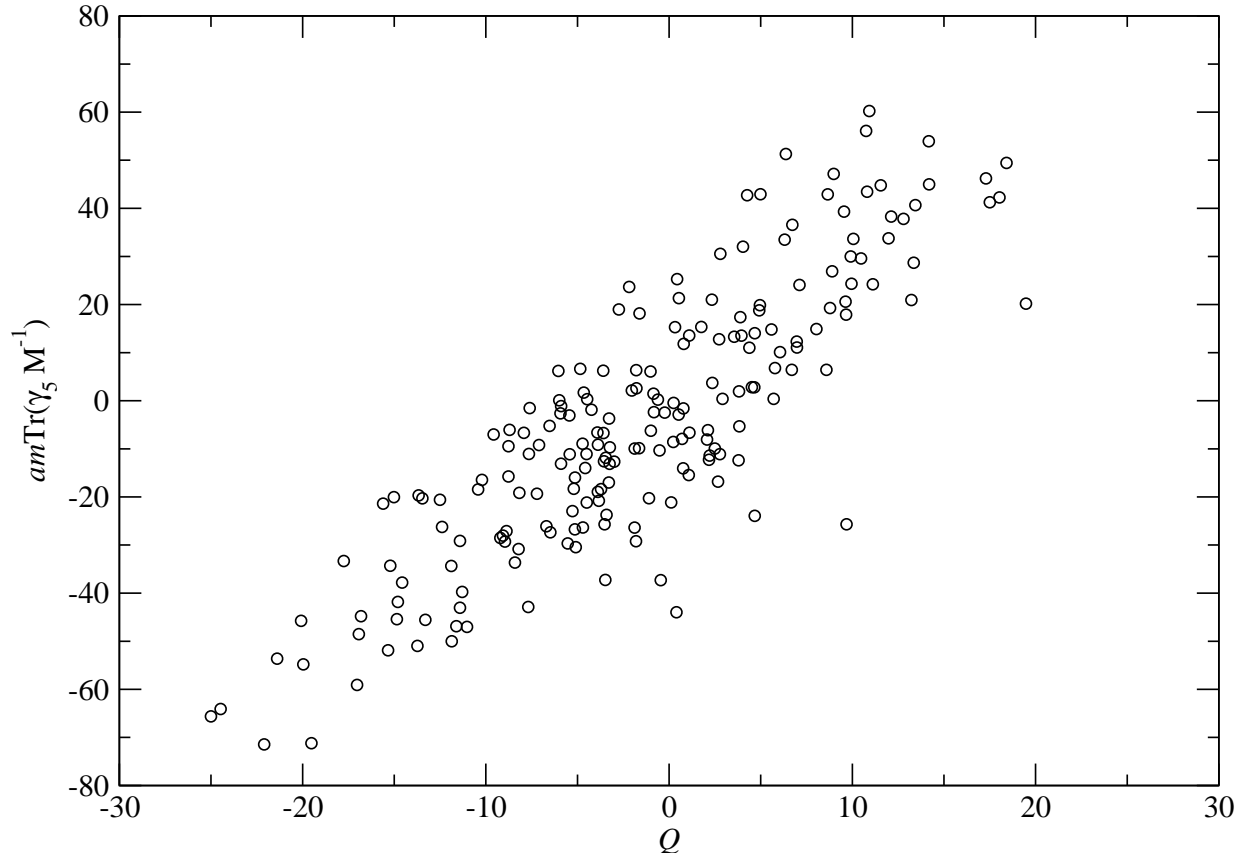


FIG. 13: Scatterplot of fermionic and gluonic definitions of topological charge on $N_f = 2+1$ -flavour $\beta = 6.76$ lattices. Light quark ($am = 0.01$) loops are used to calculate $\text{Tr}(\gamma_5 M^{-1})$.

V. STATISTICS OF DISCONNECTED CORRELATORS

Lattice QCD calculations that compute flavour singlet quantities require many more gauge configurations than those that only focus on flavour non-singlet quantities. For example, Fig. 8 shows that high statistics are required even in quenched QCD to accurately compute the D/C ratio. Although recently there have been impressive algorithmic improvements in performing unquenched lattice QCD calculations, an increase in the cost of an unquenched calculation by a factor of 10 is significant. This motivates a thorough study of the statistics of disconnected correlators.

In Fig. 14, we show a histogram of 393856 measurements (64 timeslices on 6154 quenched lattices) of the timeslice loop operator

$$L(t) \equiv \mathcal{O}_{\gamma_5 \otimes \mathbf{1}}(t) = \sum_{i \in \text{timeslice } t} [\Delta_{\gamma_5 \otimes \mathbf{1}} M^{-1}]_{ii} . \quad (32)$$

This is for the quenched data set at $\beta = 8.00$ described in Table II with valence quark mass $am = 0.05$, and shows a clear Gaussian distribution for L .

However the distribution of the disconnected correlators $D(\Delta t)$ constructed from these measurements is *not* Gaussian and standard error estimation requires some care. It is straightforward to describe the distribution of $D(\Delta t)$ in the limiting case of $\Delta t = 0$. In this case ($\Delta t = 0$), $D(\Delta t)$ is just given by the square of the loop operator $L(t)$. If independent random variables x_i (i.e. L) are Gaussian distributed:

$$P(x) = A \exp\left(-\frac{x^2}{\sigma_x^2}\right), \quad (33)$$

then $w_i = x_i^2$ have a distribution $Q(w)$:

$$Q(w) = P(x) \frac{dx}{dw} = \frac{A}{\sqrt{w}} \exp\left(-\frac{w}{\sigma_x^2}\right). \quad (34)$$

Note that the domain of $Q(w)$ is $w \geq 0$. This is consistent with the observed distribution of quenched disconnected correlator measurements D at $\Delta t = 0$ in Fig. 15.

In the region of interest, $0 < \Delta t < \Delta t_{\max}$ (with $\Delta t_{\max} \approx 15$), $L(t)$ and $L(t + \Delta t)$ are correlated non-trivially and the mean $\bar{D}(\Delta t) > 0$. In Fig. 16, the distribution of $D(\Delta t = 2)$ is clearly seen to have asymmetric tails.

Consider two Gaussian-correlated variables x and y with the same variance σ^2 . They have the joint probability distribution

$$P(x, y) = \kappa \exp\left[-(Ax^2 + Ay^2 + 2Bxy)\right]. \quad (35)$$

Changing variables to $z_i = x_i y_i$ and $\theta_i = \arctan(y_i/x_i)$ we get the joint probability for z and θ :

$$\begin{aligned} \tilde{Q}(z, \theta) &= P(x, y) \left| \frac{\partial x \partial y}{\partial z \partial \theta} \right| \\ &= \kappa \exp\left[-\left(\frac{2Az}{\sin(2\theta)} + 2Bz\right)\right] \left| \frac{1}{\sin 2\theta} \right|. \end{aligned} \quad (36)$$

Integrating out θ , treating positive and negative z regions separately (for each it suffices to integrate from zero to $\pm\pi/4$ and multiply by 4), we get

$$\begin{aligned} Q(z) &\equiv 2 \int_0^{\pi/4} d\theta \tilde{Q}(z, \theta) \\ &= 8\kappa \exp(-2Bz) \int_0^{\pi/4} d\theta \exp\left[-\left(\frac{2Az}{\sin(2\theta)}\right)\right] \left(\frac{1}{\sin(2\theta)}\right) \\ &= 4\kappa \exp(-2Bz) K_0(2A|z|), \end{aligned} \quad (37)$$

where $K_0(z)$ is a modified Bessel function of the second kind. This agrees nicely with, for example, $D(\Delta t = 2)$ measurements for the quenched $\beta = 8.00$, $am = 0.05$ ensemble data, shown in Fig. 16.

We see that in the case of $\Delta t \rightarrow \text{large}$, $D(\Delta t) \rightarrow 0$ and $B \rightarrow 0$. Equation (35) then factorises into separate x and y parts and

$$\tilde{Q}(z, \theta) = P(x)P(y) \left| \frac{\partial x \partial y}{\partial z \partial \theta} \right|. \quad (38)$$

As expected, we get

$$Q(z) = 4\kappa K_0(2A|z|). \quad (39)$$

This is consistent with the measured quenched disconnected correlators at large time separation. Fig. 17 shows these correlators for $\Delta t = 20$ together with a plot of the modified Bessel function form (39).

In all cases the most likely measurement is $D(\Delta t) = 0$, irrespective of the mean. Clearly the signal we are trying to resolve in taking the mean over disconnected correlator measurements comes from the asymmetry in the distribution, which is induced by the exponential factor in (37). When the mean disconnected correlator is small the distribution is almost symmetric and a large proportion of the signal comes from the tails of the distribution. The number of data points in the tails of the distribution many standard deviations from the mean is far greater than in a Gaussian distribution (Table VII) and act as a great lever arm on the mean itself. When Δt is large, both $D(\Delta t)$ and $C(\Delta t)$ are small and consequently the D/C ratio experiences large fluctuations.

All of this is in marked contrast to the statistics of the connected correlator, the histograms of which are less peaked and have less pronounced tails (Fig. 19). Another difference is obvious — up to differences in the asymmetry, the width of the distribution of disconnected correlator measurements remains approximately constant with respect to Δt , whereas the connected correlator distributions are of similar shape with the width roughly proportional to the mean.

The non-Gaussian nature of the distribution of disconnected correlator measurements has significant consequences for the interpretation of error estimates on these correlators, and upon derived quantities. We use bootstrap sampling methods to estimate the error on the mean of quantities of interest. Although the distribution of D is non-Gaussian, the central limit theorem ensures that the distribution of the mean \bar{D} itself is Gaussian. Given large

enough samples we should therefore be able to safely use the bootstrap resampling method to study the error on the mean using the usual confidence interval methods, but caution is called for with smaller samples.

As an example we consider the 658 configurations of the MILC coarse ensemble with $\beta = 6.76$ and sea-quark masses $am = 0.01$ and 0.05 . We measured the disconnected correlators and calculated the D/C ratio $R(\Delta t)$ as described in Section IV B. We dropped 12 configurations with trajectory index less than 100 and separated the remaining 646 into six bins of about 108 configurations each. Fig. 20 shows the D/C ratios for the subsets so defined, where the errors were calculated by bootstrap using the usual 1σ ($\sim 68\%$ confidence level) definition. We notice that, at the modest time-separation of $\Delta t = 10$, two subsets (the first and last) are nearly a standard deviation from the value obtained with all the data, and one subset (the third, highlighted with a filled circle symbol) is nearly two standard deviations from the value obtained with all 646 configurations. We can immediately trace this to the disconnected correlators (in Fig. 21, the subsets show exactly the same discrepancy in the light-quark disconnected correlator D_{qq}).

An underestimate of autocorrelation times can cause underestimation of errors, leading to an apparent disagreement between subsets of measurements. In [55] the MILC collaboration report long autocorrelation times for some $28^3 \times 96$, $a \sim 0.1\text{fm}$ ensembles, but not in the ‘coarse’ $20^3 \times 64$ ensembles. Like MILC, we found no measurable autocorrelation of the topological charge in the coarse $\beta = 6.76$, $am = 0.01, 0.05$ ensemble. The related, but more relevant quantity, the pseudoscalar singlet disconnected correlator is also suitably decorrelated. For $D_{qq}(\Delta t = 10)$ we get $\tau_{ac} = 1.09(14)$. The corresponding timeseries is shown in Fig. 22.

So the autocorrelation time is not the culprit here. It is clear from inspection that subsets of the timeseries where $D_{qq}(\Delta t)$ is particularly deviant from the mean correspond to those with a relative abundance (or deficit) of spikes or data points falling in the tails of distributions such as in Fig. 18.¹

Quenched ensembles exhibit the same features and this is particularly clear from Fig. 8. We now address the validity of the error bars on the ratio plot for the 400-configuration

¹ The points in the timeseries of $D_{qq}(\Delta t)$ measurements are of course the average of $N_t = 64$ correlated points from a distribution like Fig. 18, so the tails and peak are somewhat less severe.

subsamples. Fig. 8 shows the ratio $R = D/C$ for the first 400 configurations of each stream. The standard error for each set is computed by bootstrap, with a bin size of ten configurations. Bootstrap and jackknife give consistent error estimates. From our full 6154-configuration quenched ensemble we can make 15 bins of 400 configurations (four of the S0 bins are not shown in Fig. 8). Of these, eight have a value of $R(10)$ within its own standard error of $\overline{R(10)} = 0.28$ (the value for all 6154 configurations). Three give a value between one- and two- sigma away, and five have a value between two- and three- sigma away. Assuming the means are normally distributed (as discussed above) we would expect that only one of the fifteen bins would give a value more than 2σ from the “true” value. Although fifteen is a small number of bins, this distribution leads us to consider that the size of the error on these bins may be slightly underestimated.

If (35) is indeed the form of the distribution of loop operator measurements, then the above suggests that fitting the histogram of disconnected correlator measurements to (37) may be a useful method of extracting $D(\Delta t) = \langle z \rangle$. From (35) we easily calculate that

$$\sigma_x^2 = \sigma_y^2 \equiv \langle x^2 \rangle = \frac{A}{A^2 - B^2} \quad (40)$$

and

$$\langle xy \rangle = \frac{1}{2} \frac{-B}{A^2 - B^2}. \quad (41)$$

From the Gaussian histogram of loop operator measurements one can extract the overall normalization κ , and the width of the Gaussian puts a constraint on A and B in the form of (40), such that there remains effectively one parameter to fit to extract $\langle z \rangle$ with (41). The advantage may be that such a fit would depend less on the fluctuating tails of the distribution than the average does. We leave evaluation of this method for future work.

VI. NUMBER OF CONFIGURATIONS NEEDED

Flavour singlet lattice spectroscopy is difficult mainly because of the difficulty in getting precise determinations of the pseudoscalar disconnected correlators — disconnected correlators are far more sensitive to fluctuations in the sea than connected correlators. Furthermore the pseudoscalar quark loop operator is a measure of the topological charge which is known to be plagued with long autocorrelation times [55].

Distribution:	Normal	$P[D(\Delta t = 10)]$	$K_0(z)$	$P[D(\Delta t = 20)]$
1σ	0.317311	0.210280	0.208994	0.208147
2σ	0.045500	0.061705	0.061829	0.061289
3σ	0.002700	0.019172	0.019639	0.019606
4σ	0.000063	0.006297	0.006460	0.006751
5σ	5.73303e-07	0.002232	0.002170	0.002272
6σ	1.97318e-09	0.000779	0.000740	0.000779
7σ	2.55962e-12	0.000322	0.000255	0.000297
8σ	1.22125e-15	0.000145	0.000088	0.000104
9σ		0.000046	0.000031	0.000038
10σ		0.000025	0.000011	0.000025

TABLE VII: The integrated fraction of data occurring within a radius of multiples of the standard deviation σ from the mean. Columns two and four are analytic normal (Eq. 33) and modified Bessel (Eq. 39) distributions, respectively. Columns three and five are the observed distribution of $D(\Delta t = 10)$ and $D(\Delta t = 20)$ for 393856 measurements on quenched lattices.

We treat this work as a first step toward a more systematic exploration of pseudoscalar flavour singlets with staggered quarks. Results such as those depicted in Figures 20 and 8 and the difficulty in fitting indicate that far more configurations are necessary.

On average, over an ensemble, the error on the $\gamma_5 \otimes \mathbf{1}$ loop operator is independent of timeslice t . A consequence of this is that the product

$$\mathcal{O}_{\gamma_5 \otimes \mathbf{1}}(t) \mathcal{O}_{\gamma_5 \otimes \mathbf{1}}(t + \Delta t), \quad (42)$$

and hence the disconnected correlator $D(t)$, has an error that is roughly constant in t while the size of the correlator decreases over many orders of magnitude as t increases. See, for example, Fig. 7.

Since the gauge contribution to the statistical error of the disconnected correlator scales as $1/\sqrt{N_{\text{cfg}}}$, it is straightforward to estimate the number of configurations needed to resolve the light-light disconnected correlator (for example) out to some time-separation t to a given precision. We use the $\beta = 6.76$, $am = 0.01, 0.05$ MILC ensemble, which has 658 configuration separated by 6 trajectories. We have further grouped the lattices into bins of 10 lattices (thus eliminating 8). So with 3900 trajectories the gauge error on $D_{qq}(t)$ with

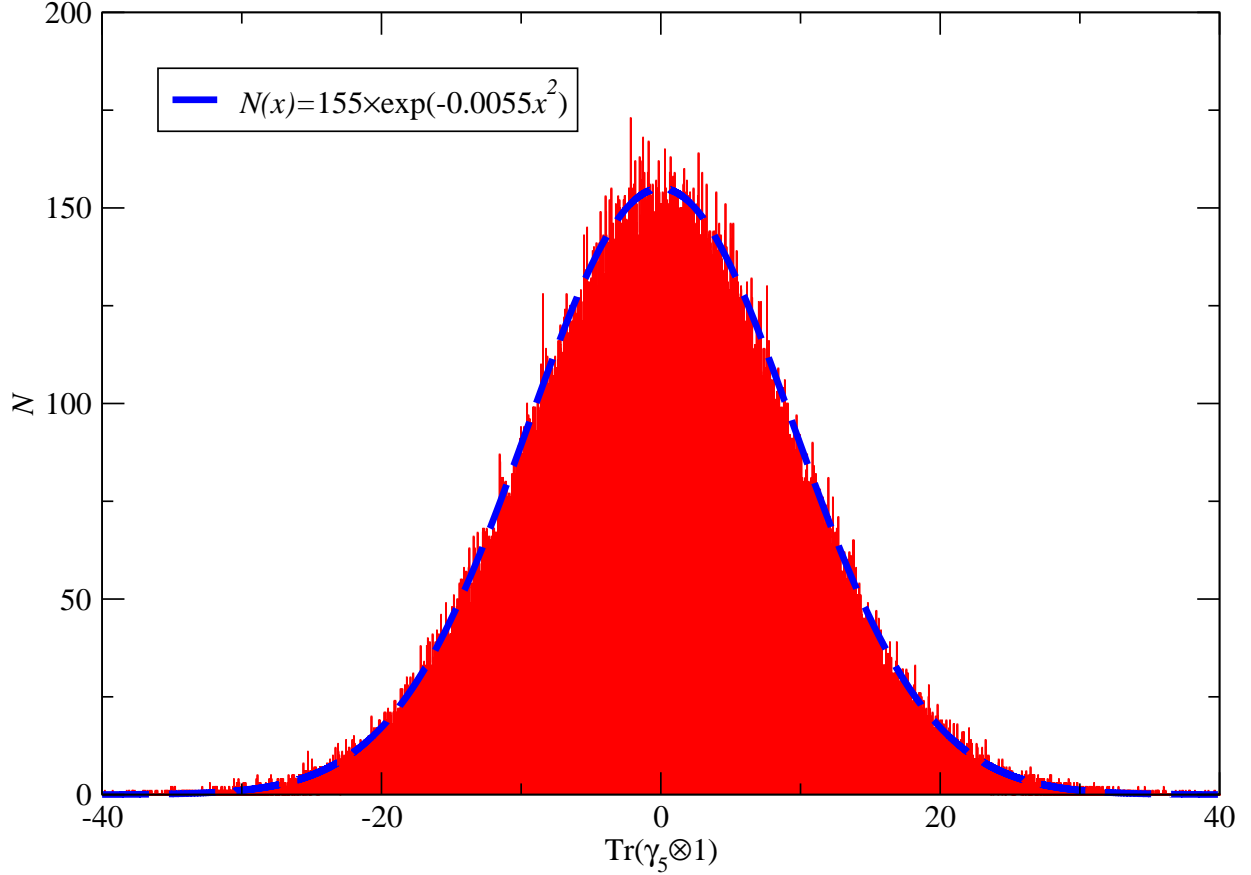


FIG. 14: Histogram of 393856 $\text{Tr}\gamma_5 \otimes \mathbf{1}$ measurements. Analytic curve is an approximation rather than a fit.

our normalization is roughly 10^{-5} , independent of t (see Fig. 4.) In Fig. 24 we use the obtained values of $D_{qq}(t)$ to estimate the number of trajectories needed for various values of precision e as a function of time separation. The dotted horizontal line represents the current 3900 trajectories, showing that we currently have 20% resolution only out to $t = 10$ and 10% resolution out to $t = 8$.

It is feasible with modern computational resources to produce ensembles using similar parameters with $\sim 2 \times 10^4$ trajectories. The position of the dashed horizontal line represents the precision one hopes to derive from these extended statistics. We hope that D_{qq} would be resolvable to 20% precision to $t = 15$ and to 10% precision to $t = 11$. The use of anisotropic lattices may be useful in allowing more time slices where the signal is bigger than the noise [72, 73]. However, the tuning of anisotropic lattice actions is non-trivial for unquenched lattice QCD calculations.

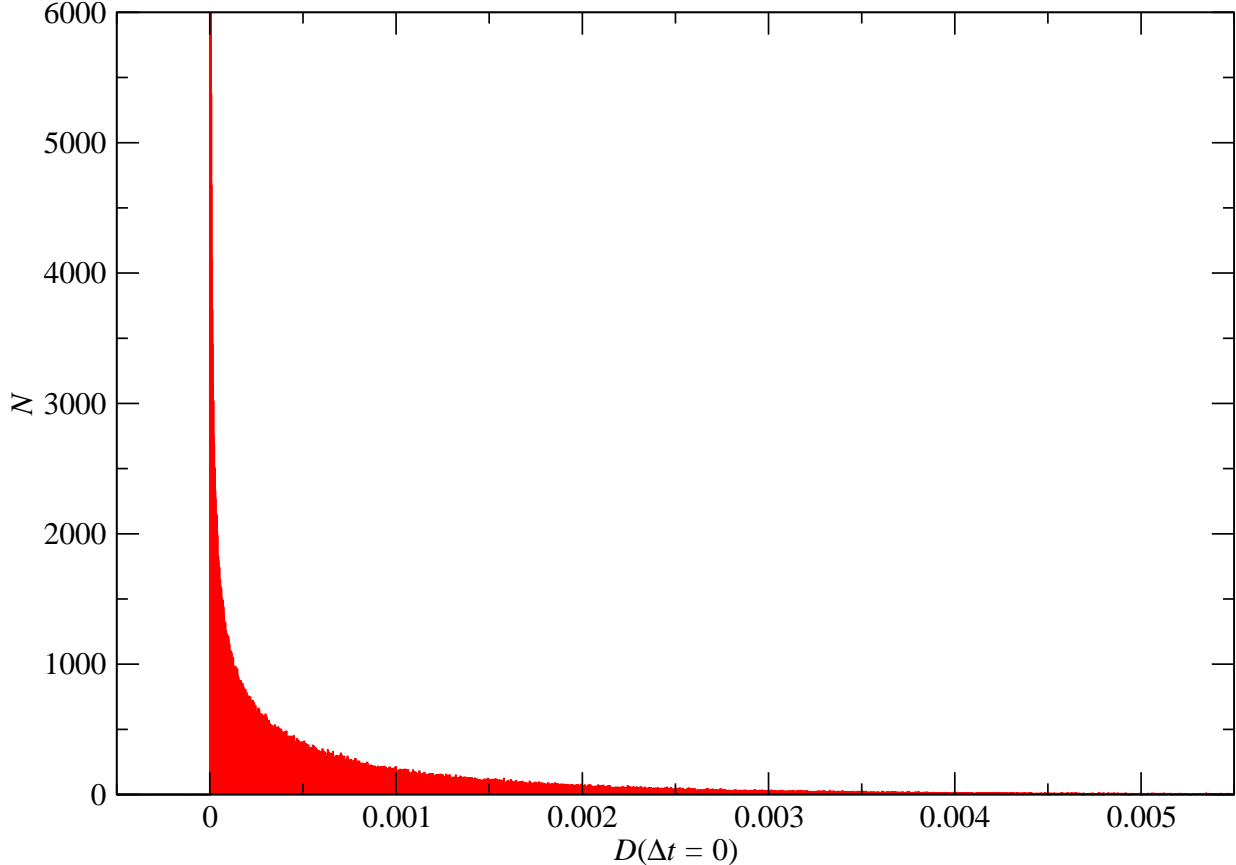


FIG. 15: Histogram of $D(\Delta t = 0)$ measurements, and a curve generated with Equation 34.

The issue of autocorrelation times has been found not to be a problem at the current lattice spacing. In the event of future work on finer lattices — a necessary step for controlling taste-breaking effects — care should be taken. However, the MILC collaboration report in [55] that topological charge autocorrelation times grow with fermion mass, so targeting lighter quark masses should help ease the problem. We are concerned with correlations of the density of $\text{Tr}\Delta_{\gamma_5 \otimes \mathbf{1}} M^{-1}$ between timeslices. The success of MILC's method of subdividing large lattices for dealing with slow topological modes suggests that autocorrelation of the topological charge density on timeslices is likely to be less of a problem than that of total topological charge.

VII. CONCLUSIONS

We have investigated a number of different algorithms to compute the disconnected diagrams required for the correlators for the singlet pseudoscalar mesons. We found that the

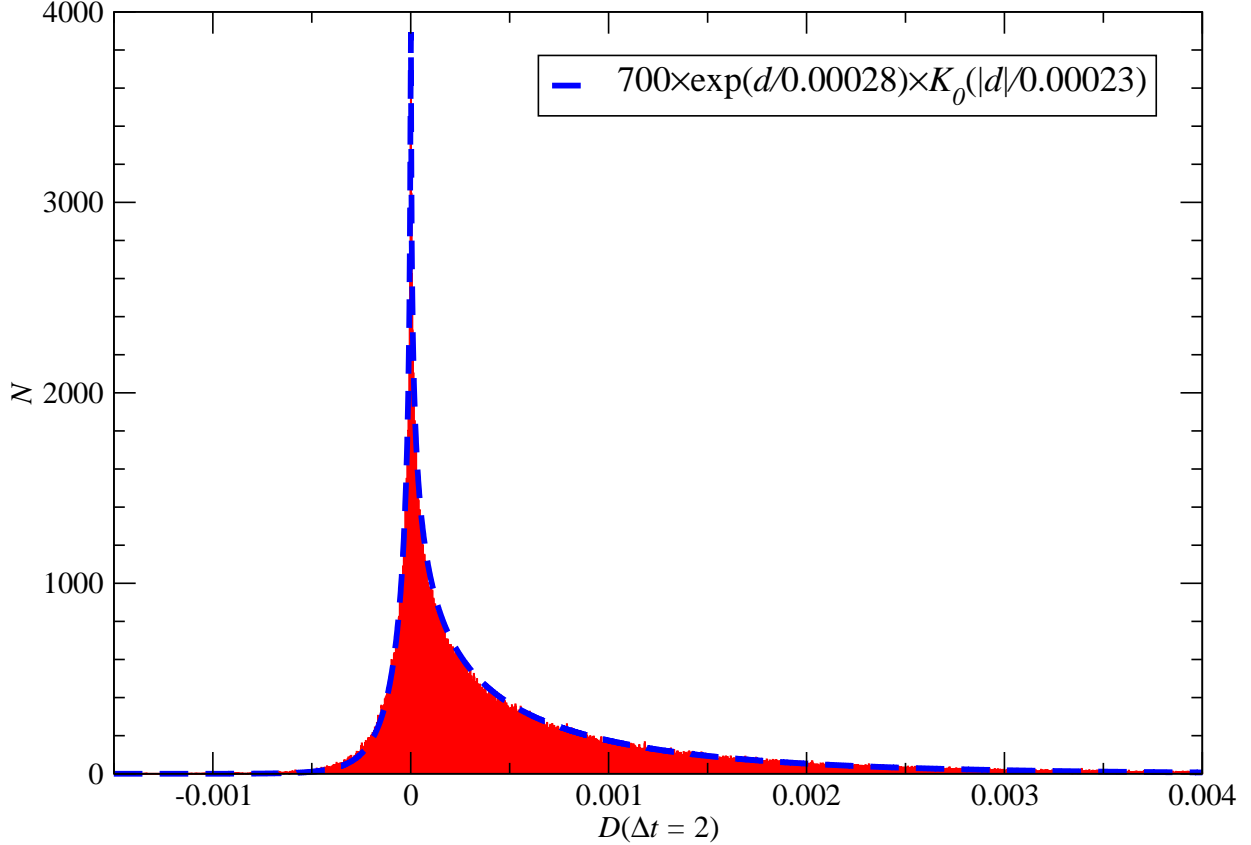


FIG. 16: Histogram of 393856 $D(\Delta t = 2)$ measurements on 6154 quenched lattices, and a curve generated with Equation 37.

algorithm proposed by Venkataraman and Kilcup [9] was the most efficient for our purposes.

Our results for the ratio of disconnected to connected diagrams (Fig. 12) do not really show a convincing difference between the quenched (10) and unquenched (9) theories. At large time separations the error on the ratio becomes large and it is not clear that it asymptotes at 1. This is in contrast to the work by Venkataraman and Kilcup [9] where the difference between quenched QCD and unquenched QCD for the ratio was clear. It is clear that higher statistics are needed for a definite conclusion on the large-time behaviour of the ratio of the disconnected to connected correlator, as well as to extract reliable masses.

We have started to study the effect of the mixing between light and strange interpolating operators. This is an essential part of the physics of the η and η' meson. The older unquenched calculations using the clover and Wilson fermion action [74], that were done with quark masses that were heavier than half the strange quark mass, produced results consistent with quenched QCD calculations for the majority of quantities. This suggested

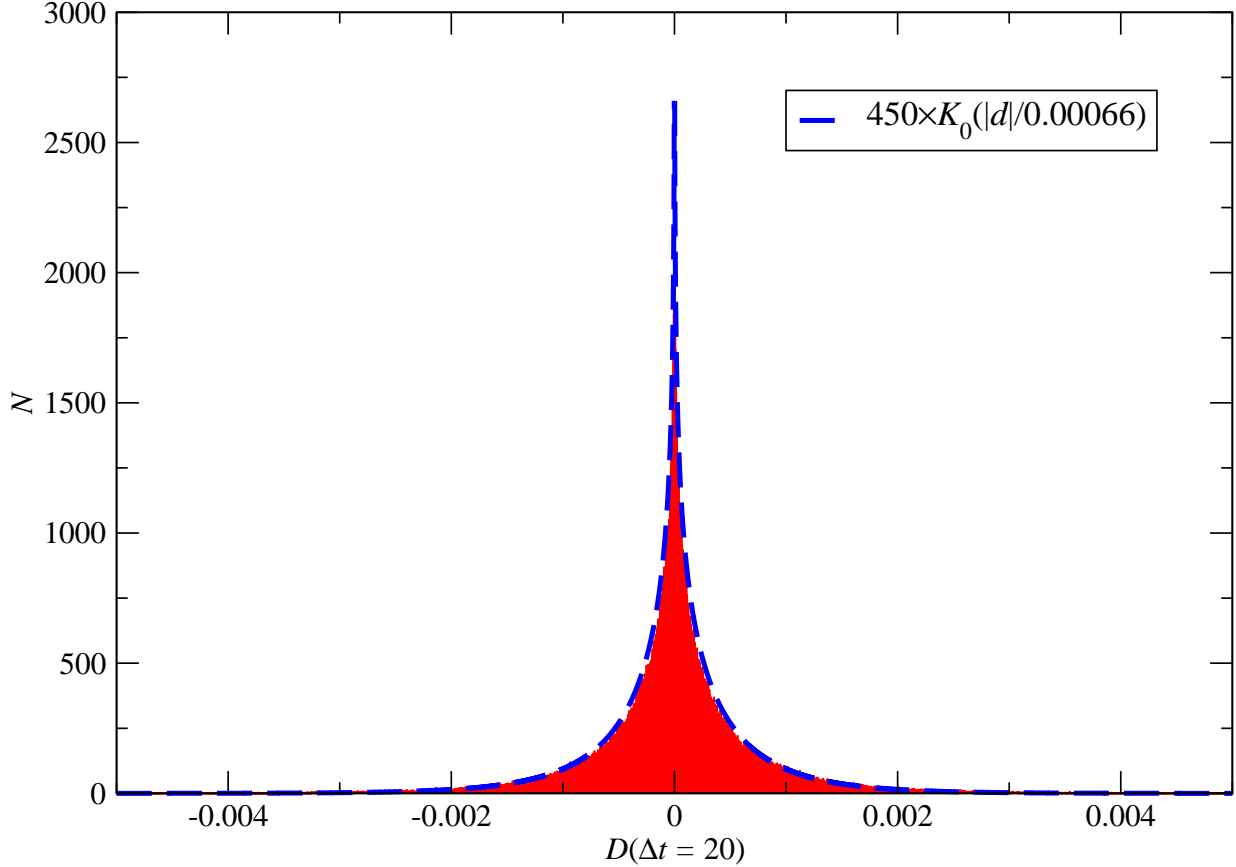


FIG. 17: Histogram of $D(\Delta t = 20)$ measurements, and a plot of a curve generated from Equation 39, the theoretical distribution of the product of two completely uncorrelated Gaussian variables.

that the strange quark would not play a significant role in the dynamics of $2 + 1$ -flavour calculations. However the strange quark clearly plays an important role in the physics of the η and η' mesons.

The correlators of the singlet pseudoscalar meson are closely related to eigenvalues of the quark operator [75]. This calculation has been done at a lattice spacing of 0.12 fm. The calculation of the eigenvalues of the Asqtad improved staggered fermion operator in quenched QCD at a lattice spacing of 0.09 fm, by Follana et al. [76], do not show convincing clustering of the eigenvalues into quartets. However, the clustering of the eigenvalues for the HISQ improved staggered action is convincing. This is some evidence that the computation of the spectroscopy of flavour singlet pseudoscalar mesons may require gauge configurations with finer lattice spacing than used here.

Although this lattice calculation has not produced the spectacular agreement with exper-

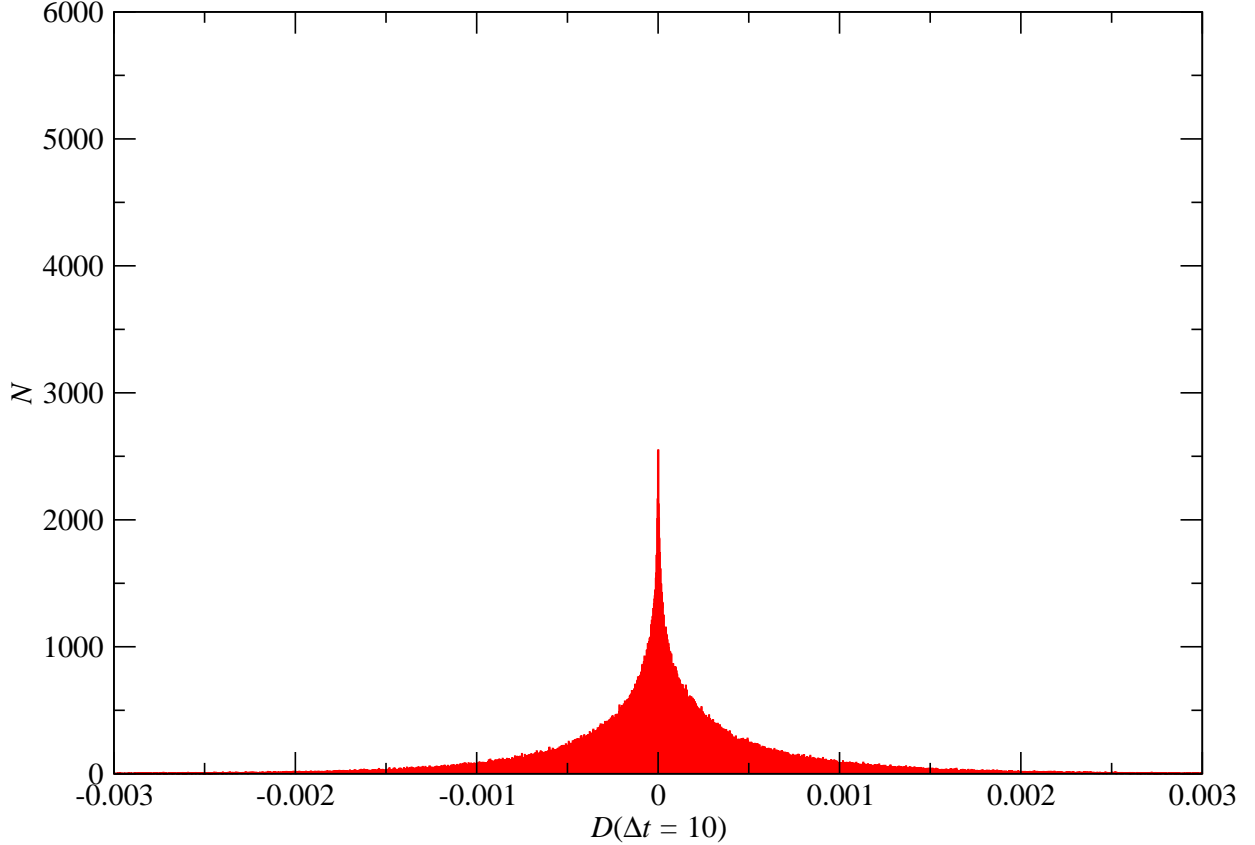


FIG. 18: Histogram of 393856 $D(\Delta t = 10)$ measurements on 6154 quenched lattices.

iment that other parts of the improved staggered program have achieved [13, 14], we have not yet seen any “show stoppers”. We are currently generating additional configurations to increase the statistics and in order to go to a finer lattice spacing.

ACKNOWLEDGEMENTS

We are grateful to the ULgrid project of the University of Liverpool for computer time. We thank Chris Michael, Christine Davies, Claude Bernard, Greg Kilcup, Steve Sharpe, Zbyszek Sroczynski, Steve Miller, and Tommy Burch for discussions.

We thank Robert Edwards and Balint Joo for help with Chroma [47]. We thank the MILC collaboration for making available their gauge configurations. This work was in part based on the MILC collaboration’s public lattice gauge theory code (see

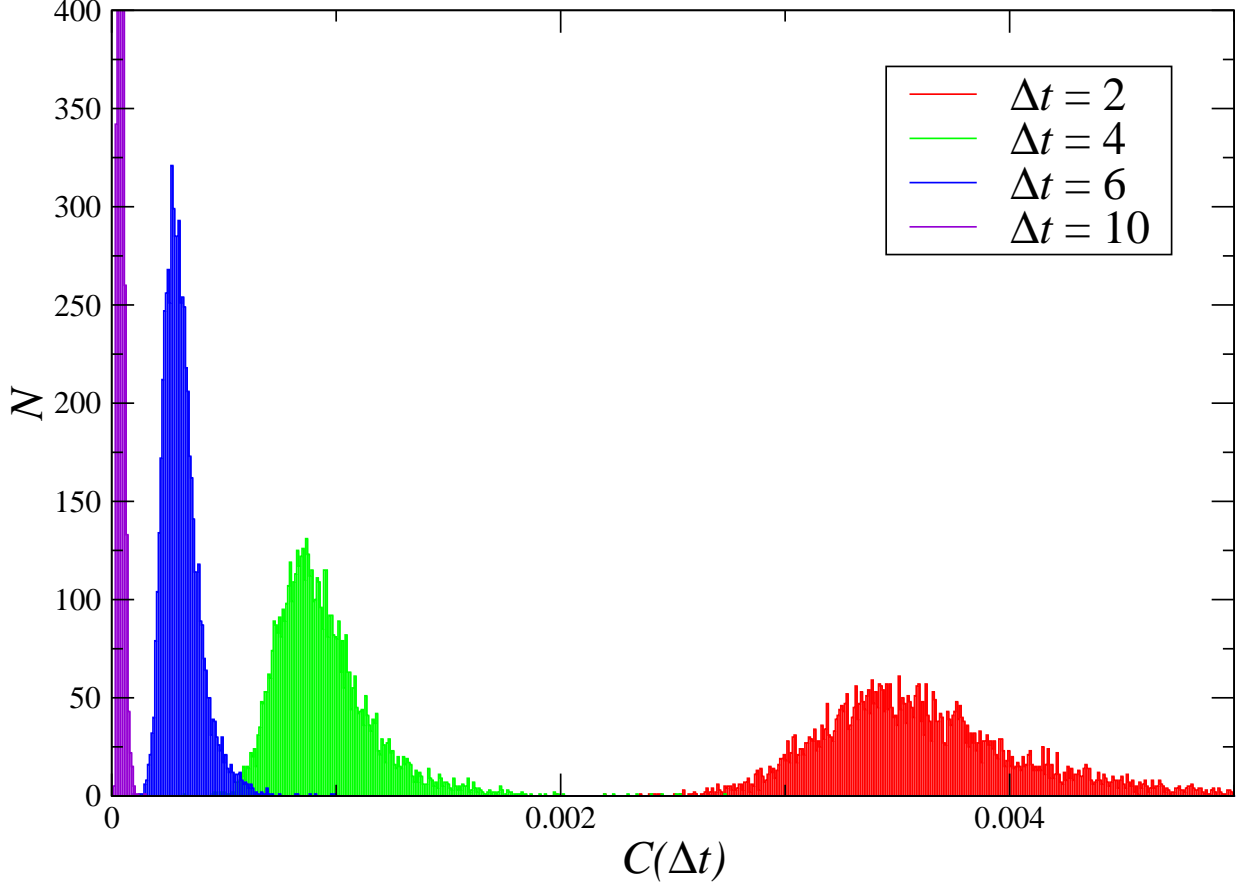


FIG. 19: Histogram of connected singlet pseudoscalar ($\gamma_5 \otimes \mathbf{1}$) measurements with $am = 0.05$ on 6154 $\beta = 8.00$ quenched lattices.

<http://physics.utah.edu/~detar/milc.html>)

-
- [1] E. Witten, Nucl. Phys. **B156**, 269 (1979),
 - [2] G. Veneziano, Nucl. Phys. **B159**, 213 (1979),
 - [3] S. Itoh, Y. Iwasaki, and T. Yoshie, Phys. Rev. **D36**, 527 (1987),
 - [4] UKQCD, C. McNeile and C. Michael, Phys. Lett. **B491**, 123 (2000), hep-lat/0006020,
 - [5] TXL, T. Struckmann *et al.*, Phys. Rev. **D63**, 074503 (2001), hep-lat/0010005,
 - [6] CP-PACS, V. I. Lesk *et al.*, Phys. Rev. **D67**, 074503 (2003), hep-lat/0211040,
 - [7] K. Schilling, H. Neff, and T. Lippert, Lect. Notes Phys. **663**, 147 (2005), hep-lat/0401005,
 - [8] MILC, T. A. DeGrand and U. M. Heller, Phys. Rev. **D65**, 114501 (2002), hep-lat/0202001,
 - [9] L. Venkataraman and G. Kilcup, (1997), hep-lat/9711006,

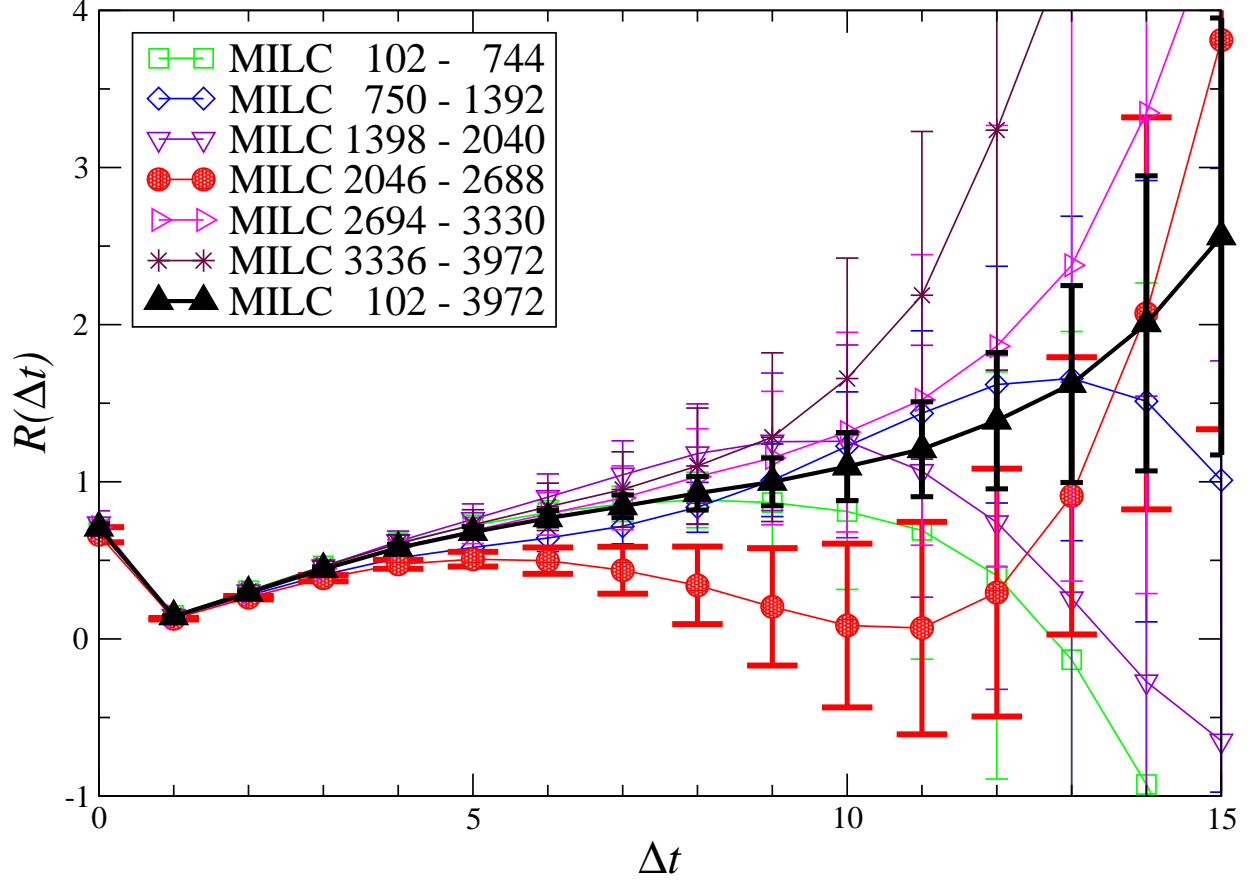


FIG. 20: Binned D/C ratio for $\beta = 6.76$ $am = 0.01, 0.05$.

- [10] J. B. Kogut, J. F. Lagae, and D. K. Sinclair, Phys. Rev. **D58**, 054504 (1998), hep-lat/9801020,
- [11] H. Fukaya and T. Onogi, Phys. Rev. **D70**, 054508 (2004), hep-lat/0403024,
- [12] JLQCD, S. Aoki *et al.*, (2006), hep-lat/0610021,
- [13] HPQCD, C. T. H. Davies *et al.*, Phys. Rev. Lett. **92**, 022001 (2004), hep-lat/0304004,
- [14] C. Aubin *et al.*, Phys. Rev. **D70**, 094505 (2004), hep-lat/0402030,
- [15] S. R. Sharpe, PoS **LAT2006**, 022 (2006), hep-lat/0610094,
- [16] S. Durr, PoS **LAT2005**, 021 (2006), hep-lat/0509026,
- [17] M. Creutz, Phys. Lett. **B649**, 230 (2007), hep-lat/0701018,
- [18] M. Creutz, (2007), arXiv:0708.1295 [hep-lat],
- [19] J. F. Donoghue, E. Golowich, and B. R. Holstein, Camb. Monogr. Part. Phys. Nucl. Phys. Cosmol. **2**, 1 (1992),
- [20] T. Feldmann and P. Kroll, Phys. Scripta **T99**, 13 (2002), hep-ph/0201044,
- [21] A. Hasenfratz, (2005), hep-lat/0511021,

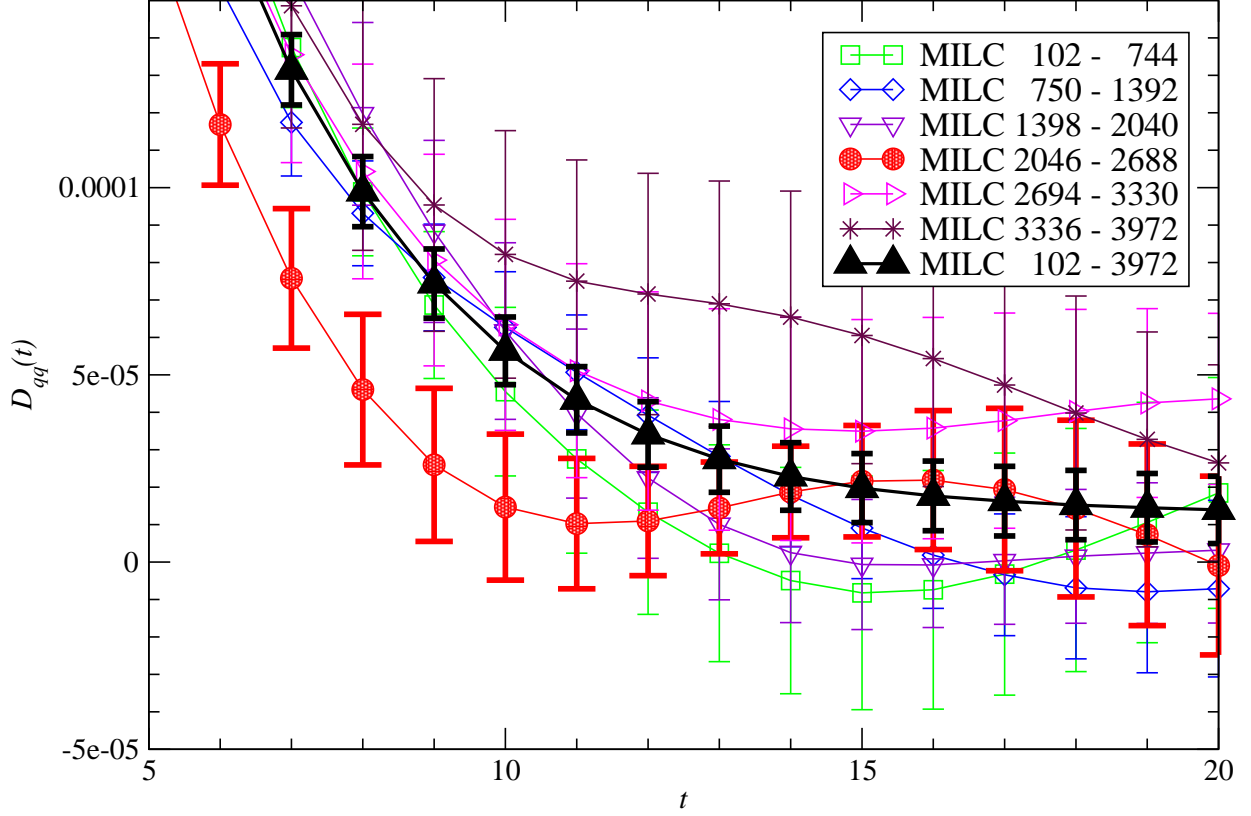


FIG. 21: Binned D_{qq} correlators for $\beta = 6.76$ $am = 0.01$.

- [22] C. J. Morningstar and M. J. Peardon, Phys. Rev. **D56**, 4043 (1997), hep-lat/9704011,
- [23] C. J. Morningstar and M. J. Peardon, Phys. Rev. **D60**, 034509 (1999), hep-lat/9901004,
- [24] UKQCD, A. Hart and M. Teper, Phys. Rev. **D65**, 034502 (2002), hep-lat/0108022,
- [25] Particle Data Group, W. M. Yao *et al.*, J. Phys. **G33**, 1 (2006),
- [26] UKQCD, C. McNeile and C. Michael, Phys. Rev. **D63**, 114503 (2001), hep-lat/0010019,
- [27] M. Luscher and U. Wolff, Nucl. Phys. **B339**, 222 (1990),
- [28] T. Burch *et al.*, Phys. Rev. **D74**, 014504 (2006), hep-lat/0604019,
- [29] T. Burch *et al.*, Phys. Rev. **D73**, 094505 (2006), hep-lat/0601026,
- [30] UKQCD, C. McNeile and C. Michael, Phys. Lett. **B642**, 244 (2006), hep-lat/0607032,
- [31] UKQCD, A. Hart, C. McNeile, C. Michael, and J. Pickavance, Phys. Rev. **D74**, 114504 (2006), hep-lat/0608026,
- [32] C. W. Bernard *et al.*, Phys. Rev. **D64**, 054506 (2001), hep-lat/0104002,
- [33] MILC, K. Orginos and D. Toussaint, Phys. Rev. **D59**, 014501 (1999), hep-lat/9805009,
- [34] MILC, K. Orginos, D. Toussaint, and R. L. Sugar, Phys. Rev. **D60**, 054503 (1999), hep-

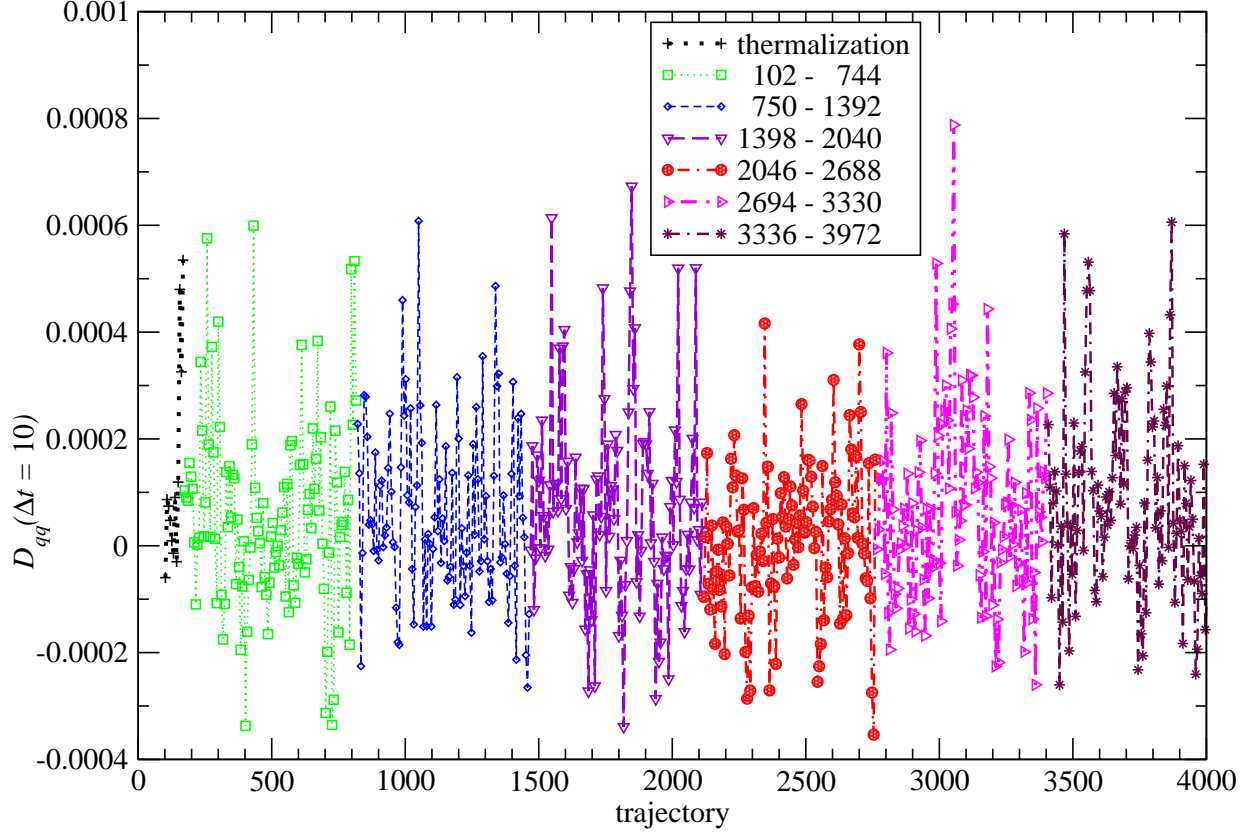


FIG. 22: Timeseries of D_{qq} correlator measurements (averaged over timeslices) for $\beta = 6.76$ $am = 0.01$.

lat/9903032,

[35] K. Orginos, R. Sugar, and D. Toussaint, Nucl. Phys. Proc. Suppl. **83**, 878 (2000), hep-lat/9909087,

[36] G. P. Lepage, Phys. Rev. **D59**, 074502 (1999), hep-lat/9809157,

[37] H. Kluberg-Stern, A. Morel, O. Napoly, and B. Petersson, Nucl. Phys. **B220**, 447 (1983),

[38] M. F. L. Golterman, Nucl. Phys. **B273**, 663 (1986),

[39] S.-J. Dong and K.-F. Liu, Phys. Lett. **B328**, 130 (1994), hep-lat/9308015,

[40] W. Wilcox, (1999), hep-lat/9911013,

[41] F. Farchioni, G. Muenster, and R. Peetz, Eur. Phys. J. **C38**, 329 (2004), hep-lat/0404004,

[42] S. Bernardson, P. McCarty, and C. Thron, Comput. Phys. Commun. **78**, 256 (1993),

[43] E. B. Gregory, A. C. Irving, C. McNeile, S. Miller, and Z. Sroczynski, PoS **LAT2005**, 083 (2006), hep-lat/0509193,

[44] UKQCD, C. Michael and J. Peisa, Phys. Rev. **D58**, 034506 (1998), hep-lat/9802015,

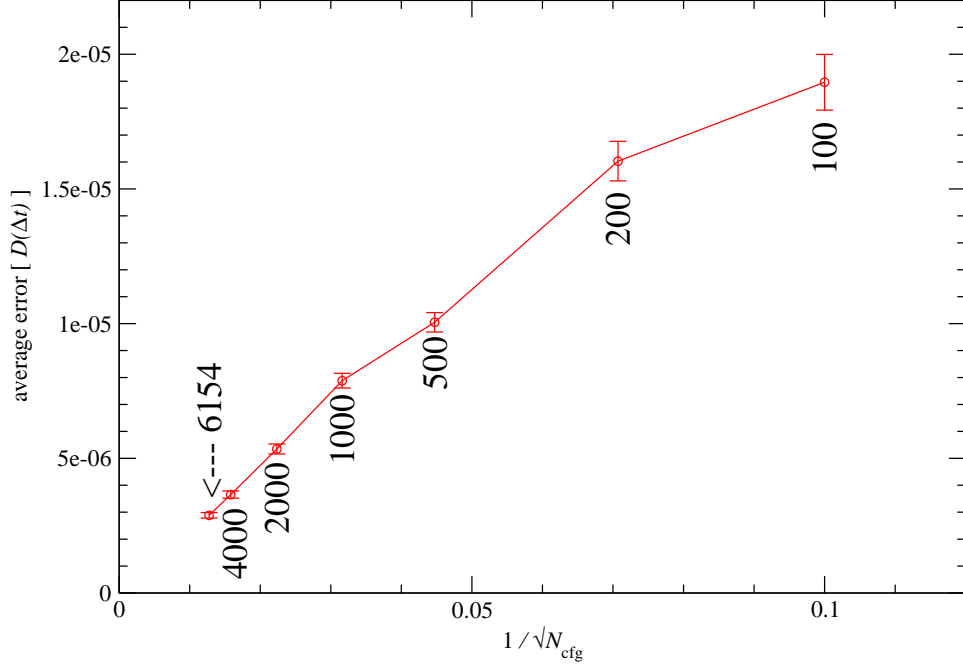


FIG. 23: Error on $D(\Delta t)$, averaged over Δt , for $\beta = 8.00$ quenched configurations with $am = 0.05$, as a function of $1/\sqrt{N_{\text{cfg}}}$.

- [45] J. Foley *et al.*, Comput. Phys. Commun. **172**, 145 (2005), hep-lat/0505023,
- [46] E. B. Gregory, A. Irving, C. McNeile, S. Miller, and Z. Sroczynski, Nucl. Phys. Proc. Suppl. **153**, 139 (2006), hep-lat/0511038,
- [47] SciDAC, R. G. Edwards and B. Joo, Nucl. Phys. Proc. Suppl. **140**, 832 (2005), hep-lat/0409003,
- [48] C. W. Bernard and M. F. L. Golterman, Phys. Rev. **D46**, 853 (1992), hep-lat/9204007,
- [49] W. A. Bardeen, E. Eichten, and H. Thacker, Phys. Rev. **D69**, 054502 (2004), hep-lat/0307023,
- [50] Y. Kuramashi, M. Fukugita, H. Mino, M. Okawa, and A. Ukawa, Phys. Rev. Lett. **72**, 3448 (1994),
- [51] W. A. Bardeen, E. Eichten, and H. B. Thacker, Phys. Rev. **D70**, 117502 (2004), hep-lat/0405020,
- [52] ALPHA, M. Guagnelli, R. Sommer, and H. Wittig, Nucl. Phys. **B535**, 389 (1998), hep-lat/9806005,
- [53] G. M. Shore, Nucl. Phys. **B744**, 34 (2006), hep-ph/0601051,
- [54] B. Lucini and M. Teper, JHEP **06**, 050 (2001), hep-lat/0103027,

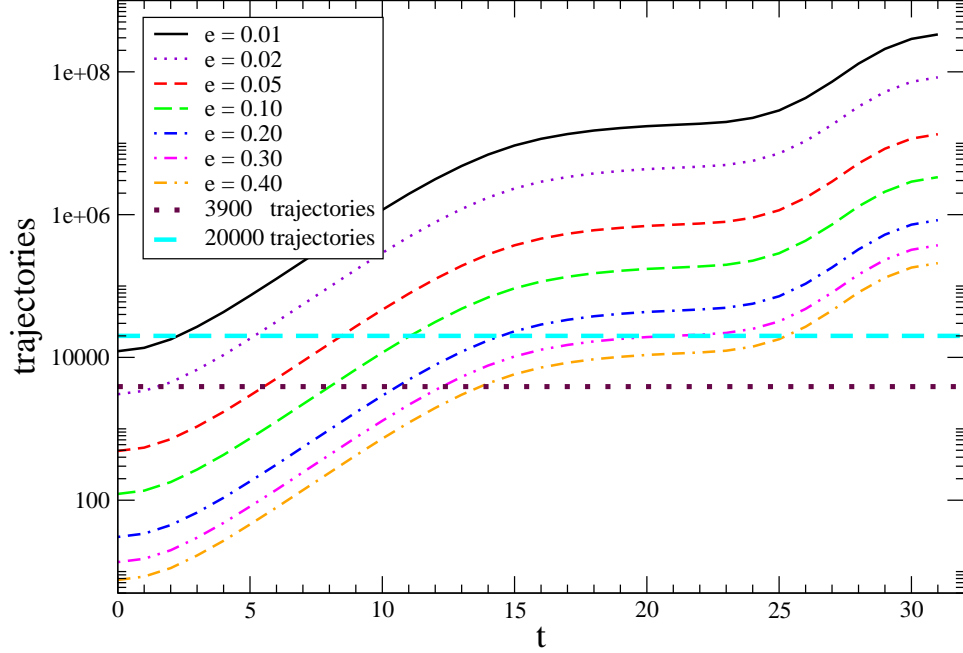


FIG. 24: Estimated trajectories needed for improved precision of $D_{qq}(t)$ for $\beta = 6.76$ $am = 0.01$ $20^3 \times 64$ lattices, where $e(t) \equiv \overline{\sigma_{D_{qq}}}/D_{qq}(t)$.

- [55] C. Bernard *et al.*, Phys. Rev. **D68**, 114501 (2003), hep-lat/0308019,
- [56] L. Del Debbio, L. Giusti, and C. Pica, Phys. Rev. Lett. **94**, 032003 (2005), hep-th/0407052,
- [57] S. Durr, Z. Fodor, C. Hoelbling, and T. Kurth, JHEP **04**, 055 (2007), hep-lat/0612021,
- [58] S. R. Sharpe, Phys. Rev. **D69**, 034504 (2004), hep-lat/0308009,
- [59] J. F. Lagae and K. F. Liu, Phys. Rev. **D52**, 4042 (1995), hep-lat/9501007,
- [60] XLF, K. Jansen *et al.*, Phys. Lett. **B624**, 334 (2005), hep-lat/0507032,
- [61] C. Aubin and C. Bernard, Phys. Rev. **D68**, 034014 (2003), hep-lat/0304014,
- [62] S. Prelovsek, Phys. Rev. **D73**, 014506 (2006), hep-lat/0510080,
- [63] C. W. Bernard, C. DeTar, Z. Fu, and S. Prelovsek, PoS **LAT2006**, 173 (2006), hep-lat/0610031,
- [64] J. Smit and J. C. Vink, Nucl. Phys. **B286**, 485 (1987),
- [65] M. F. Atiyah and I. M. Singer, Annals Math. **87**, 484 (1968),
- [66] B. Alles *et al.*, Phys. Rev. **D58**, 071503 (1998), hep-lat/9803008,
- [67] B. Billeter, C. DeTar, and J. Osborn, Phys. Rev. **D70**, 077502 (2004), hep-lat/0406032,
- [68] MILC, <http://physics.utah.edu/~detar/milc.html>.
- [69] T. A. DeGrand, A. Hasenfratz, and T. G. Kovacs, Nucl. Phys. **B505**, 417 (1997), hep-

- lat/9705009,
- [70] A. Hasenfratz and F. Knechtli, Phys. Rev. **D64**, 034504 (2001), hep-lat/0103029,
 - [71] B. Alles, M. D’Elia, A. Di Giacomo, and C. Pica, Phys. Rev. **D74**, 094503 (2006), hep-lat/0604007,
 - [72] R. Morrin, A. O. Cais, M. Peardon, S. M. Ryan, and J.-I. Skullerud, Phys. Rev. **D74**, 014505 (2006), hep-lat/0604021,
 - [73] L. Levkova, T. Manke, and R. Mawhinney, Phys. Rev. **D73**, 074504 (2006), hep-lat/0603031,
 - [74] UKQCD, C. R. Allton *et al.*, Phys. Rev. **D65**, 054502 (2002), hep-lat/0107021,
 - [75] H. Neff, N. Eicker, T. Lippert, J. W. Negele, and K. Schilling, Phys. Rev. **D64**, 114509 (2001), hep-lat/0106016,
 - [76] HPQCD, E. Follana, A. Hart, C. T. H. Davies, and Q. Mason, Phys. Rev. **D72**, 054501 (2005), hep-lat/0507011,